ORIGINAL PAPER

The influence of the heterogeneity of rock mass for surrounding rock stability evaluation of a tunnel

Guofeng Li[1] · Mingming He[1,2,3] · Yue Bai[4]

Abstract

In this study, we reviewed the influence of various heterogeneity factors of rock mass on the displacement of the tunnel. We derived the critical deformation formula and proposed the stability evaluation method via the elastoplastic analytical solution of a circular tunnel. The traffic tunnel of the *Sanhekou* hydro-junction project was taken as an example to establish the heterogeneous rock mass finite difference method model. A new method is proposed to obtain the most basic heterogeneous rock mass parameters, and evaluated the stability of the heterogeneous rock mass tunnel. The results showed that when the weak interlayer is randomly distributed, the deformation of the wall increases with the decrease in the average value of the parameters, and it is significantly affected by its standard deviation. The core of the stability evaluation process of the heterogeneous rock mass tunnel is to obtain the radius of the plastic zone and the distribution of weak interlayer. If the distribution characteristics of the interlayer are not determined, the critical deformation may be appropriately reduced by 15% to evaluate the stability of the tunnel. We also verified the reliability of the stability evaluation method by monitoring the 2# diversion tunnel of the *Zipingpu* hydraulic project.

Keywords Heterogeneous · Rock mass · Tunnel · Stability evaluation

Introduction

Evaluating the stability of rock mass around underground excavations is a difficult and significant task during tunnel construction (Jiang et al. 2021a, b). It is closely related to the safety of the working space and sustainability and economics of the project (Muhammad et al. 2019; Liu et al. 2015; Liu et al. 2021; Li et al. 2021). However, rock mass contains numerous discontinuities, such as fissures, fractures, joints, faults, dikes, and shear zones, which result in complex mechanical properties, such as discontinuity (Yan et al. 2018), heterogeneity (Abdul et al. 2019), anisotropy (Zhang et al. 2019), and non-linear (Ong and Choo 2018). To overcome the tunnel stability evaluation problem on the heterogeneous surrounding rock mass, accurate description of the deformation and stress characteristics of the heterogeneous rock mass is necessary.

Furthermore, numerical analysis has irreplaceable superiority (Li et al. 2019) over analytical methods, physical experimental methods, field test methods, and so on. The numerical methods rely on the heterogeneous model and parameters. The heterogeneous parameters refer to the basic physical and mechanical parameters (density, deformation modulus, Poisson ratio, cohesion, frictional angle) of the rock mass that is heterogeneously distributed to different locations. The heterogeneous model refers to a numerical simulation calculation model established according to the heterogeneous distribution of rock mass. The heterogeneity of rock mass parameters mainly considers rock mass grading using empirical formula methods (Bieniawski et al. 1978; Bieniawski 1973; Barton 2002; Hoek and Brown 1980). Heterogeneous models are often researched using various methods, such as separating rock mass layer (Chen et al.

✉ Mingming He
  hemingming@xaut.edu.cn

1 State Key Lffigaboratory of Eco-Hydraulics in Northwest Arid Region of China, University of Technology, Xi'an 710048, China

2 Shaanxi Key Laboratory of Loess Mechanics and Engineering, Xi'an University of Technology, Xi'an 710048, China

3 State Key Laboratory of Geohazard Prevention and Geoenvironment Protection, Chengdu University of Technology, Chengdu 610059, China

4 SCEGC NO.3 Construction Engineering Group Company Limited, Xi'an 710054, China

2019), using structural plane element (Zhang et al. 2017), adopting random fracture distribution (Ado et al. 2019), and cellular automata (Ma and Tan 2005; Pi et al. 2015).

Researchers have conducted various studies on heterogeneous models and parameters but they often ignore the importance of evaluating the tunnel stability of heterogeneous rock mass. Currently, there are a few reports on the methods of evaluating tunnel stability of heterogeneous rock mass. Stability evaluation methods of homogeneous rock mass tunnels, according to the different indicators, can be summarized into four categories: the strength criterion index method (Gao et al. 2016), the tunnel deformation index method (Li and Zhu 2013), the catastrophe theory method (Wang et al. 2019), and the indirect evaluation method of characterizing surrounding rock stability with support structure safety (Li et al. 2014; Liu et al. 2015). In practical engineering, the homogeneous stability evaluation methods are adopted for evaluating the stability of heterogeneous tunnels, which may be risky and unsafe in some cases (Ma et al. 2009). Therefore, it is imperative to propose a new stability evaluation method for heterogeneous tunnels or to modify the homogeneous tunnel stability methods.

This paper is structured as follows. In the "Review of factors on heterogeneity of rock mass" section, we discuss the influence of the heterogeneity factors of rock mass, such as width, number, position and distribution of the weak interlayer, and distance between the interlayer and the tunnel, on the displacement of the tunnel based on the ideal heterogeneous rock mass tunnel model. In the "Tunnel stability evaluation methods" section, we derive the critical deformation formula of the tunnel and propose the stability evaluation method for the heterogeneous tunnel via the elastoplastic analytical solution of a circular tunnel. In the "Case study" section, we obtain the heterogeneous parameters, establish a heterogeneous model, and analyze and evaluate the stability of the heterogeneous tunnel by considering the traffic tunnel of the *Sanhekou* hydro-junction project as an example. In the "Discussion and application" section, we verify the feasibility of the stability evaluation method by monitoring 2# diversion tunnel of the *Zipingpu* hydraulic project. Finally, in the "Conclusion" section, we present the conclusions of this study.

## Review of factors on heterogeneity of rock mass

The discontinuities embedded in the surrounding rock mass of an underground tunnel are critical for the stability of the surrounding rock mass, especially in tunnel engineering (Zhang et al. 2017). Furthermore, the heterogeneities also play an important role in the stability of the surrounding rock mass in tunnel engineering. A geological simplified model of surrounding rock mass after tunnel excavation is shown in Fig. 1a. In addition to the influence of rock mass

properties, the stability of the tunnel is also affected by the adjacent weak interlayer. Various factors, such as the distance between the interlayer and the wall, the thickness and the number of the interlayer, and the relative position of the interlayer and the tunnel, are worth considering. Therefore, in this section, we focus on the effects of these factors on the deformations of the tunnel wall after excavation.

A city gate shape tunnel cross-section is adopted, as shown in Fig. 1b. The range of the model is set by considering the influence range of tunnel stress and deformation, which is four times the tunnel diameter. In this study, we build and mesh the model, and calculate and verify the same by the FLAC^{3D} software package. The primary information of the tunnel model is presented in Table 1. To simplify the calculation, all supporting measures are not considered. A heterogeneous distribution of weak interlayers is set on the right wall. It is assumed that the weak interlayer is vertically distributed on the outside of the right wall with equal thickness. The element thickness is 1 m and the element size is 0.5–1.0 m. The total number of nodes and elements after meshing are 9339 and 6024, respectively.

In Table 1, H-4 D and H + 5 D are the distance from the top and bottom of the model to the ground surface, respectively. The initial stress field is generated by the weight gradient of the rock mass. The uniform stress boundaries are applied on the top (P1) and bottom (P2) of the model according to the tunnel buried depth. The gradient stress boundaries are applied at the sides (P3 and P4) of the model by the lateral pressure coefficient. The initial stress field is identical to the actual stress environment; thus, its calculation is balanced in only one step and the calculation speed and accuracy of the subsequent excavation simulation can be accelerated. The mechanical parameters of the rock mass and the weak interlayer are selected according to the grade IV rock and grade V rock, respectively. The mechanical parameters of the rock mass and weak interlayer are presented in Table 2 (Zhang et al. 2017). To study the effect of the weak interlayer on the deformation of the side wall after tunnel excavation, the primary analysis scheme for the tunnel of heterogeneous rock mass is designed, as presented in Table 3.

In Table 3, the displacement responses of the wall after excavation are studied based on heterogeneous distribution and equivalent homogeneous distribution of the surrounding rock mass. The first group scheme mainly considers a weak interlayer, with different combinations of the thickness of the interlayer and the distance between the interlayer and tunnel wall. The second group scheme mainly considers the heterogeneous distribution of surrounding rocks, under the same conditions of the ratio of weak interlayer (number of interlayers × width of the interlayer/total influence width), and with various combinations of soft hard intervals of rock mass and interlayer. The third group scheme mainly
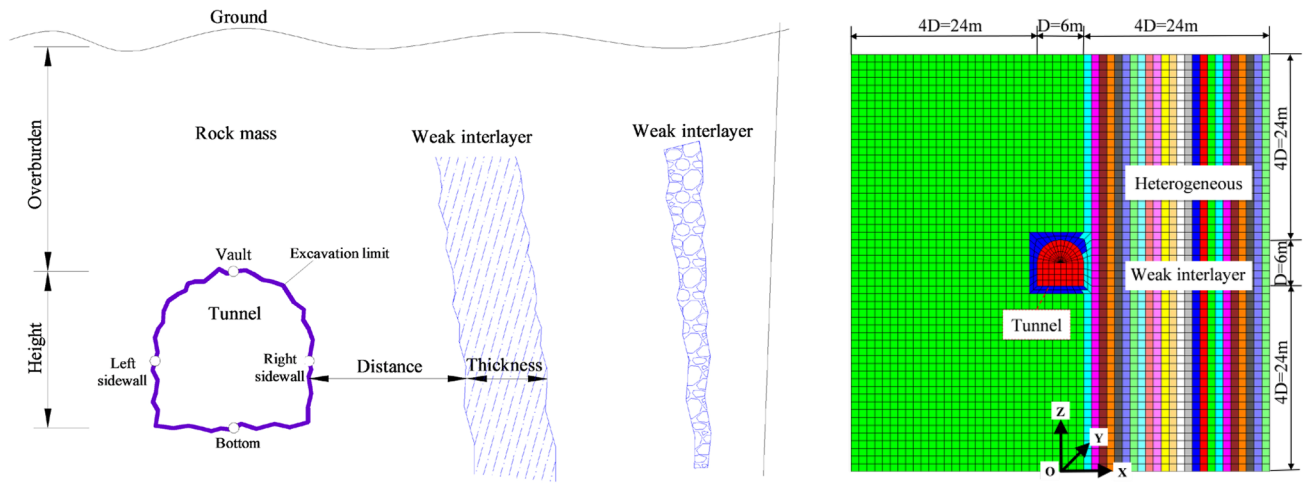
(a) Geological model and key points

(b) Numerical model and model size
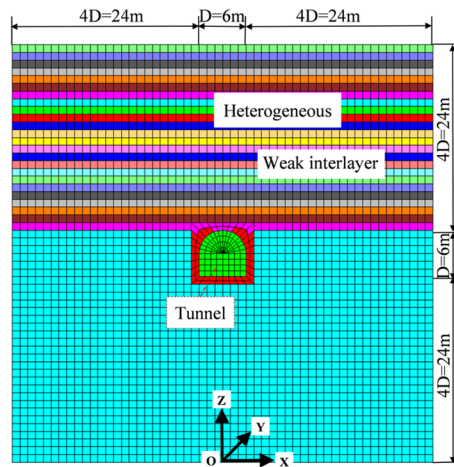
(c) Numerical model and model size

Fig. 1 Tunnel model of the heterogeneous rock mass

considers the thickness of the weak interlayer at 1 m; the tunnel excavation is studied with various combinations on different interlayers and distance between the interlayer and the wall. The fourth group scheme uses the *Randbetween() function* of *Microsoft Excel* to generate 10 groups × 24 m random numbers in the deformation modulus (0.1 ~ 3.0

Table 1 Primary information of the analyzed tunnel model

Item	Description
Cross-section	Rectangular conduit with circular upper wall
Height	$h = D = 6.0$ m
Span	$b = D = 6.0$ m
Overburden	$H = 100.0$ m
Lateral pressure coefficient	$\lambda = 1.0$
Model size	$\triangle X = \triangle Z = 54.0$ m, $\triangle Y = 1.0$ m, the range of influence is 4D
Boundary condition	Top, Z = 54.0 Apply P1 = − (H-4D) ρg Bottom, Z = 0.0 Fix-Z Apply P2 = − (H + 5D) ρg Plane X = ±27.0 Fix-X Apply P3 = (P2 + ρg•Z) λ Plane Y = 0.0, Y = 1.0 Fix-Y Apply P4 = P3

Table 2 Mechanical parameters of the rock mass and weak interlayer

Material	Density, ρ (kg/m³)	Deformation modulus, E (GPa)	Poisson ratio, μ	Cohesion, c (MPa)	Frictional angle, φ (°)
Rock mass	2350	3.0	0.32	0.8	28
Weak interlayer	2150	0.1	0.40	0.6	23

GPa). The other parameters are interpolated according to the corresponding law using the *Trend() function* of *Microsoft Excel*. Among these parameters, the deformation modulus of the random sample is presented in Table 4. The equivalent homogeneous rock mass parameters are obtained by weighing the proportion of rock mass and weak interlayer.

Distance between weak interlayer and tunnel wall

When the number of weak interlayer is one, the deformation responses of the tunnel wall after excavation with various distances and thickness of the weak interlayer, under the heterogeneous distribution of surrounding rock and equivalent homogeneous distribution, are shown in Fig. 2.

Figure 2a–d show that the displacement law of the wall is similar with different weak interlayer thicknesses. The displacement of the wall gradually increases with the decrease in the distance. First, the deformation of the right wall increases slowly. Further, when the distance is less than 4.0 m, deformation turning occurs and increases rapidly. When the distance is less than 3.0 m, deformation turning of the vault and bottom occurs and increase rapidly. However, the deformation of the left wall first decreases at 2.0 m, then the transition occurs and increases. The displacement increments of each key point are presented in Table 5. When a weak interlayer is present on one side of the wall, this side wall is first affected, the vault and the arch bottom follow. The deformation of another side wall is affected only when the weak interlayer is closer to the wall. The displacement increment is also reduced in turn. The displacement increment of each key point increases with the increase in the thickness of the weak interlayer. With the increase in the thickness of the weak interlayer, the heterogeneous deformation (HED) of the left-side wall is always smaller than the homogeneous deformation (HOD). When the thickness is 1.0, 2.0, 3.0, and 4.0 m, the reduction ratio of HED relative to HOD on the left-side wall is 4.2, 6.6, 10.5, and 16.7%, respectively. It is dangerous that the heterogeneous rock mass tunnel is evaluated by the homogeneous critical deformation at this time. However, there are minimum distances in other regions. HED is greater than HOD only for distance less than the minimum distance, as presented in Table 6. The minimum distance decreases with the increase in the thickness.

Table 3 Primary analysis scheme for the tunnel of the heterogeneous rock mass

Group	Numbers of weak interlayer	Thickness(m)	Distance(m)	Scheme description
1	1	1.0	0, 1, 2, …,23	
	1	2.0	0, 1, 2, …,23	
	1	3.0	0, 1, 2, …,23	
	1	4.0	0, 1, 2, …,23	
2	12	1.0	0, 1	
	6	2.0	0, 2	
	4	3.0	0, 3	
	3	4.0	0, 4	
	2	6.0	0, 6	
3	8	1.0	0, 1,2	
	6	1.0	0, 1,2,3	
	4	1.0	0, 1,2,3,4,5	
	3	1.0	0, 1,2,…,7	
	2	1.0	0, 1,2,…,11	
4	Random sample			

Table 4 Deformation modulus (*E*) of the random sample by the analysis scheme

Distance (m)	Deformation modulus of random sample *E* (GPa)									
	1	2	3	4	5	6	7	8	9	10
0	1.10	0.70	2.70	2.80	2.80	2.00	0.70	2.30	1.90	0.80
1	2.10	2.20	1.50	1.80	1.90	2.80	1.50	3.00	0.10	1.80
2	0.40	1.90	1.40	2.00	0.10	1.90	0.30	3.00	1.10	0.20
3	2.40	0.20	2.20	2.20	2.50	0.30	2.00	1.30	0.30	2.80
4	1.80	2.60	2.80	0.80	1.40	1.60	1.00	2.40	2.60	0.80
5	2.50	0.90	2.00	2.60	1.80	0.30	0.60	1.60	1.20	1.60
6	1.00	1.50	1.70	1.10	1.30	2.20	3.00	1.80	0.90	2.40
7	1.40	1.00	2.00	2.90	0.10	1.60	1.50	0.60	1.10	2.30
8	1.60	2.50	2.70	2.70	0.20	2.30	1.10	1.10	1.40	2.80
9	0.10	0.30	2.80	2.00	2.30	0.80	2.90	2.00	0.90	1.90
10	1.00	2.30	0.80	2.70	1.00	2.50	0.50	2.40	0.30	1.50
11	1.00	2.70	1.80	2.10	0.50	1.10	2.10	0.20	2.70	0.60
12	2.90	2.50	2.00	1.30	0.40	0.60	2.70	2.10	2.80	0.10
13	1.10	2.40	1.10	1.50	0.70	2.50	0.10	1.50	2.10	0.50
14	0.70	2.40	1.80	3.00	1.60	1.20	1.70	1.30	2.20	0.90
15	2.50	2.60	3.00	2.70	1.50	0.90	2.30	2.60	1.40	0.50
16	1.60	3.00	0.30	1.40	0.60	1.00	2.70	2.90	0.90	2.90
17	2.00	1.90	0.90	2.60	0.60	0.70	1.90	0.50	2.80	0.60
18	2.60	1.00	2.40	2.60	1.60	1.00	2.40	2.20	2.60	0.60
19	0.50	0.60	2.00	1.70	2.50	0.50	1.30	0.40	2.50	1.40
20	0.20	2.30	2.70	0.10	2.40	2.50	3.00	2.30	2.80	1.70
21	1.60	0.10	1.60	1.20	2.00	0.90	2.50	0.80	1.60	1.00
22	0.30	2.00	2.00	0.50	0.70	1.50	3.00	0.50	2.40	3.00
23	1.70	0.20	0.90	1.00	1.70	0.90	1.20	1.10	3.00	2.40
Average value	1.42	1.66	1.88	1.89	1.34	1.40	1.75	1.66	1.73	1.46
Standard deviation	0.82	0.95	0.73	0.83	0.84	0.77	0.93	0.88	0.91	0.93

Figure 2e and f show that the displacement law of the tunnel wall with the interlayer thickness is similar despite the distances being different. When the weak interlayer is adjacent to the tunnel wall, the displacement of each key point increases with the increase in the weak interlayer thickness; however, the extent of increase decreases gradually. When the weak interlayer is away from the tunnel wall, the displacement of each key point does not change much with the increase in the thickness.

Thickness of weak interlayer

Considering that the ratio of the weak interlayer is 50%, with various combinations of soft and hard intervals of the rock mass and the interlayer, the effects of the number of weak interlayers, thickness, and soft and hard distributions on the displacement of the wall are shown in Fig. 3.

Figure 3 shows that, with the same number of interlayers, when the interlayer is adjacent to the wall with a soft-hard distribution, the deformation is greater than the deformation of the interlayer with non-adjacent wall and a hard-soft distribution. When the interlayer is distributed next to the wall, the displacement of each key point is gradually reduced, with the number of interlayers increasing or the thickness of the interlayer decreasing. The displacement of the right-side wall reduces and the decreasing rate is gradually reduced. This shows that the thickness of the interlayer is dominant for the soft-hard distribution interlayer. When the number of interlayers is less and the thickness is large, it has more influence on the displacement of the wall, as compared to that with the number of interlayers being more and the thickness being small. When the interlayer is not closely adjacent to the cave wall, and when the number of interlayers increases or the thickness of the interlayer decreases, the displacement of the left-side wall gradually decreases, the displacement of the remaining part gradually increases, and the displacement of the right-side wall increases. This shows that the number of interlayers is dominant for the hard-soft distribution interlayer. When the number of interlayers is more and the thickness is small, it has more influence on the displacement of the wall, compared with the number of interlayers being less and the thickness being more.

When the interlayer is adjacent to the tunnel wall, HOD is greater than HED for the left-side wall and vault, and HOD

(a) Thickness =1m

(b) Thickness =2m

(c) Thickness =3m

(d) Thickness =4m

(e) Distance =0m
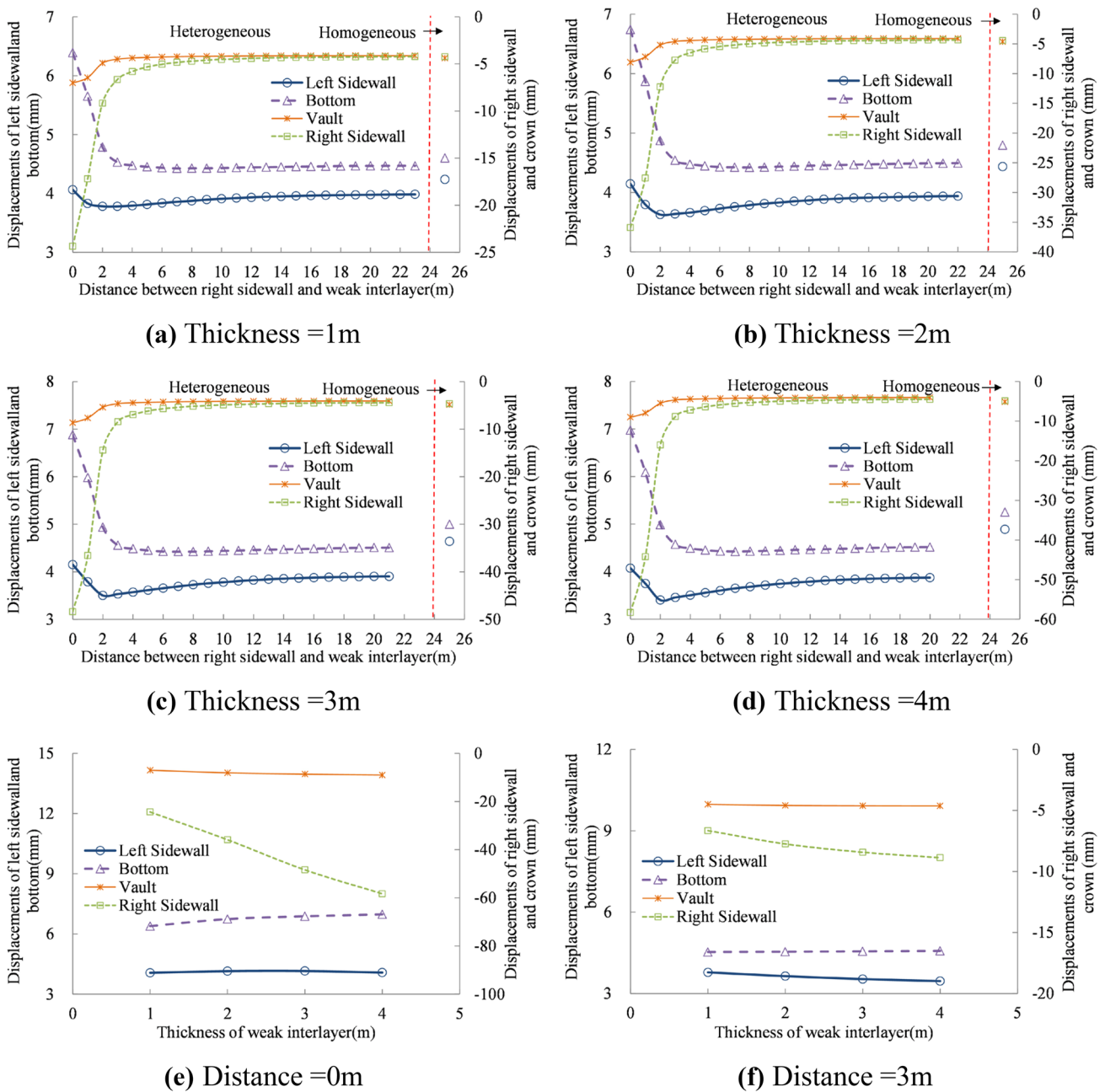
(f) Distance =3m

Fig. 2 The influence of various weak interlayers with different thickness and distance on tunnel deformation

of the right-side wall is much smaller than HED. HOD of the vault is greater than HED only when the number of interlayers is greater than four. When the interlayer is not adjacent to the wall, the homogenous deformation of most key points is greater than HED. HOD of the right-side wall is less than HED only when the number of interlayers is greater than three. When the number of weak interlayers is two, the reduction ratios of HED relative to HOD, for the vault, the left- and right-side walls, and the arch bottom, are 51.4, 57.5, 22.4, and 47.2%, respectively. When the number of weak interlayers is

three, the reduction ratios of HED relative to HOD, for the vault, the left- and right-side walls, and the arch bottom, are 49.7, 58.8, 4.6, and 46.5%, respectively. This shows that it is dangerous if the heterogeneous rock mass tunnel is evaluated by homogeneous critical deformation at this time.

Number of weak interlayer

When the thickness of the weak interlayer is 1.0 m, the number of interlayers and the distance between the interlayer

Table 5 Increment in displacement with various thicknesses of weak interlayer

Thickness (m)	Vault (mm)	Left sidewall (mm)	Right sidewall (mm)	Bottom (mm)
1.0	− 2.51	0.28	− 18.55	1.86
2.0	− 3.50	0.52	− 29.38	2.20
3.0	− 4.03	0.65	− 41.45	2.32
4.0	− 4.38	0.67	− 51.07	2.40

Table 6 Minimum distance between the weak interlayer and tunnel under the displacement of heterogeneous rock mass is greater than that under the displacement of homogeneous rock mass

Thickness (m)	Vault (m)	Left sidewall (m)	Right sidewall (m)	Bottom (m)
1.0	3.0	/	20.0	2.0
2.0	2.0	/	15.0	2.0
3.0	2.0	/	12.0	1.0
4.0	2.0	/	10.0	1.0

and the wall has different effects on the displacement of the tunnel, as shown in Fig. 4.

According to Figs. 4a–d, the effect of the number of interlayers on the displacement of the tunnel is similar with different distances; the only difference is magnitude. As the number of interlayer increases, the deformation of the left-side wall gradually decreases, and the deformation of the remaining key points gradually increases. As the distance between the interlayer and the wall increases, the effect on the displacement gradually diminishes. For an equivalent homogeneous rock mass, the displacement of each key point increases with the increase in the number of weak interlayers or the increase of the proportion of interlayer.

Figure 4e and f show that, with different number of interlayers, the influence of the distance between the interlayer and the wall on the displacement of the tunnel is similar; the only difference is magnitude. The displacement of each key point gradually increases as the distance decreases; turning occurs at a distance of 2 m, and then increases rapidly. HED is larger and smaller than HOD for the right-side and left-side walls, respectively. When the distance is less than 3.0 and 2.0 m, HED is larger than HOD for the vault and bottom, respectively. The influence of tunnel displacement is similar for both cases, i.e., for two or three interlayers with a thickness of 1 m and for a single weak interlayer with a thickness of 2 or 3 m, as presented in Table 7.

As presented in Table 7, within the effective range of tunnel excavation, for the same proportion of weak interlayers, the weak interlayer with a small number and large thicknesses has a greater influence on the tunnel. Under the condition of the existing interlayer distribution, the closer the outer interlayer is to the existing interlayer, the greater is the influence on the tunnel. For the same proportion of interlayers, HED is larger than HOD for most key points, only HED of the left-side wall is less.

Distribution of weak interlayer

For 10 groups of randomly distributed heterogeneous rock samples, the deformation law of each key point along the average deformation modulus after excavation is shown in Fig. 5a. The relation between the standard deviation of each group parameter and the average deformation modulus is as shown Fig. 5b.

Figure 5 shows that, for an equivalent homogeneous rock mass, the displacement of each key point decreases linearly with the increase in the deformation modulus. For the heterogeneous rock mass, the displacement of each key point decreases with the increase in the deformation modulus and is affected by the standard deviation. Especially for the deformation of the right-side wall, the degree of parameter

(a) Distance =0m

(b) Distance≠0m
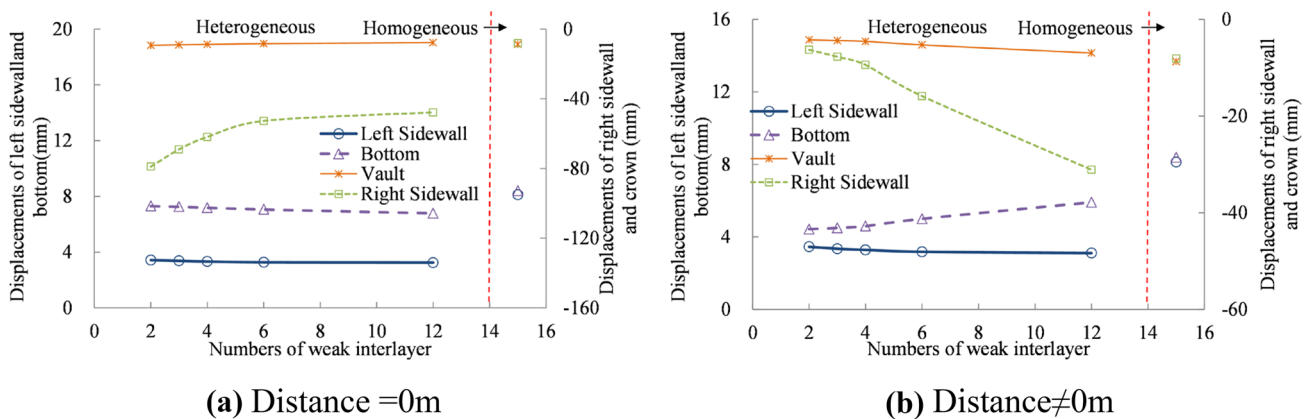
Fig. 3 The influence of the thickness of the weak interlayer on tunnel deformation

(a) Distance =0m

(b) Distance=1m

(c) Distance =2m

(d) Equivalent homogeneous rock mass

(e) Numbers =2

(f) Numbers =3
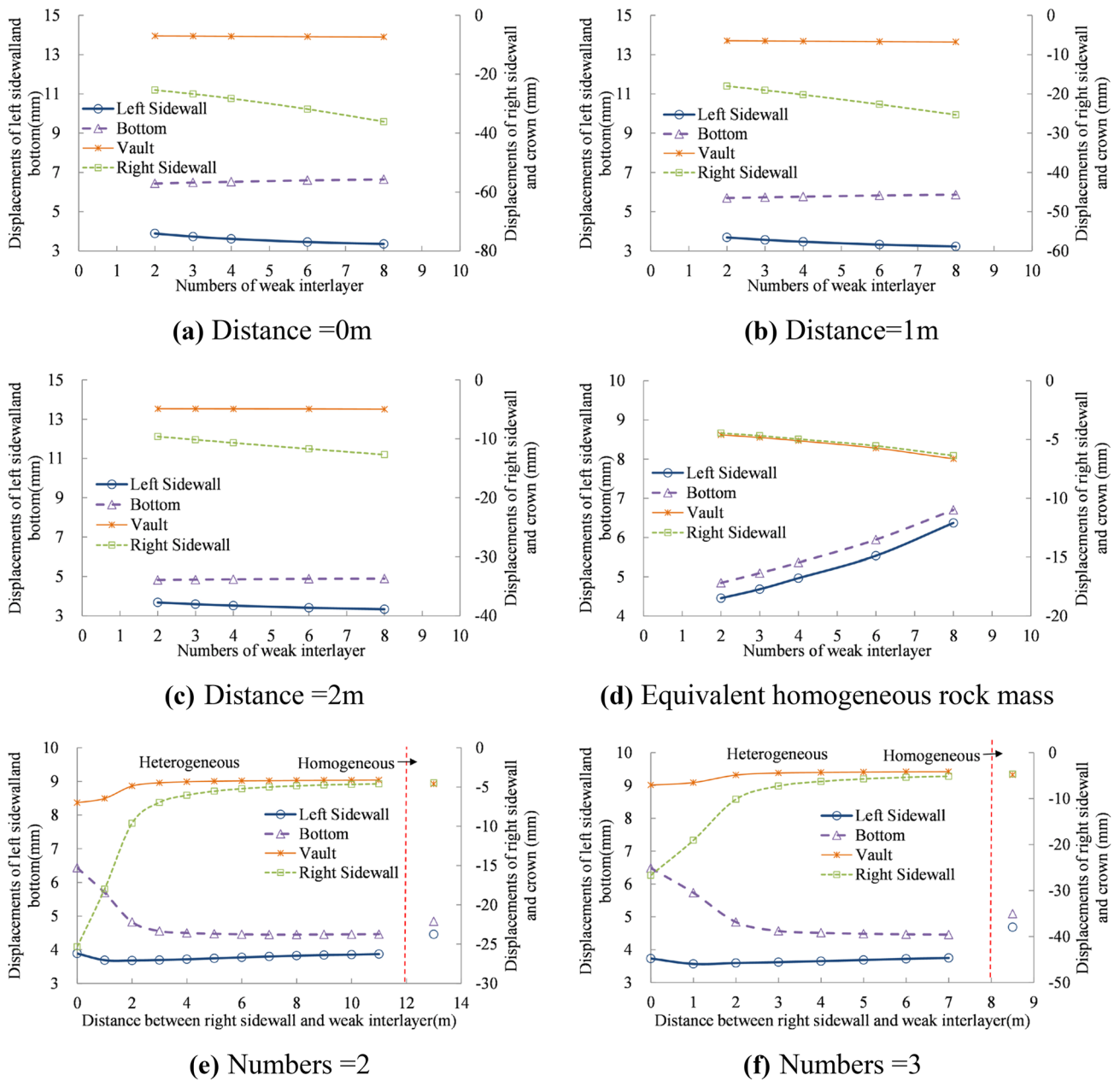
Fig. 4 The influence of the number of weak interlayer on tunnel deformation

dispersion and the displacement increases with the increase in the standard deviation. In addition, if the random rock mass is distributed in the vault, as shown in Fig. 1c, the deformation law of each key point is similar to the sidewall. It has greater influence only on the deformation of the vault and it changes with the standard deviation. Except for the

Table 7 Displacement of key points

Item	Weak interlayer		Displacement(mm)			
	Thickness (m)	Numbers	Vault	Left sidewall	Right sidewall	Bottom
Heterogeneous	2.0	1	−8.09	4.14	−35.90	6.74
	1.0	2	−7.00	3.89	−25.34	6.44
Homogeneous	2.0		−4.62	4.44	−4.44	4.80
Heterogeneous	3.0	1	−8.65	4.15	−48.39	6.88
	1.0	3	−7.05	3.73	−26.68	6.48
Homogeneous	3.0		−4.85	4.64	−4.64	4.99

Fig. 5 The influence of random weak interlayer distribution on tunnel deformation
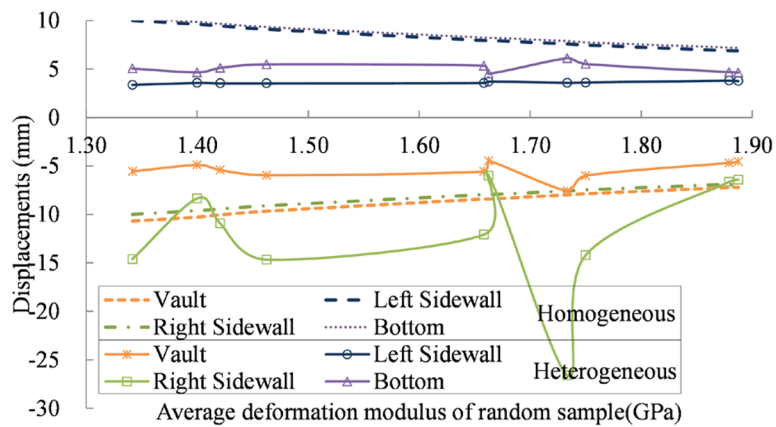
(a) Displacement with average deformation modulus
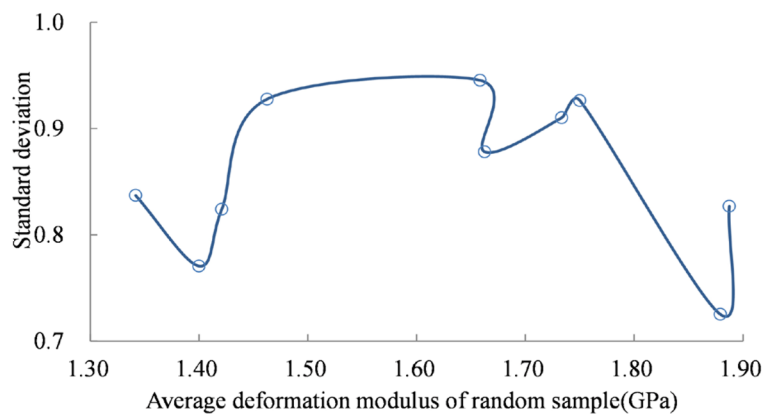
(b) Standard deviation with average deformation modulus

right-side wall, the deformation of each key point of the equivalent homogeneous rock mass is larger than that of the random heterogeneous rock mass. The deformation difference percentage for the tunnel with equivalent homogeneous and heterogeneous rock masses, for the parameter groups with smaller standard deviations, is presented in Table 8.

Other factors

Dispersion of rock mass parameters

The dispersion degree of the surrounding rock parameters may have a certain impact on the deformation of the tunnel.

So, two schemes are proposed to study the impact. The surrounding rock parameters remain unchanged and the weak interlayer parameters are changed for the scheme #1, while the assumption is just the opposite for the scheme #2. The deformation modulus of the two schemes are presented in Table 9, and other parameters are interpolated according to the corresponding law by using the *Trend( ) function*. The deformation of the surrounding rock with different dispersions is shown in Fig. 6, when the distance is 0 m, the thickness is 1.0 m, and the number of weak interlayers is 6. The displacement of each key point increases with the decrease of the interlayer parameters for the scheme #1. And the change trend increases sharply when the relative ratio

Table 8 Deformation difference percentage

Group	Average value of E (GPa)	Standard deviation	Vault	Left sidewall	Right sidewall	Bottom
6	1.40	0.77	52.3%	62.9%	13.1%	52.8%
8	1.66	0.88	46.8%	53.5%	24.6%	45.2%
3	1.88	0.73	35.2%	44.7%	3.5%	35.1%
4	1.89	0.83	37.1%	45.3%	6.7%	35.8%

Table 9 Analysis scheme for the dispersion of deformation modulus (E) of the heterogeneous rock mass

scheme	Item	1	2	3	4	5	6
#1	Rock mass (GPa)	3.00					
	Weak interlayer (GPa)	0.01	0.05	0.10	0.50	1.00	1.50
	Dispersion (%)	0.33	1.67	3.33	16.67	33.33	50.00
#2	Rock mass (GPa)	3.00	6.00	9.00	12.00	15.00	18.00
	Weak interlayer (GPa)	0.10					
	Dispersion (%)	3.33	1.67	1.11	0.83	0.67	0.56

is less than 16.67%. For the equivalent homogeneous rock mass, the deformation of each key point is not much different. However, the displacement linearly decreases with the increase of the rock mass parameters for the scheme #2. And when the dispersion (1.67) of the two schemes is the same, the deformation of each key point of the scheme #1 is about twice that of the scheme #2 for the equivalent homogeneous rock mass. Furthermore, the deformation of the right-side wall of the scheme #2 is about three times that of the scheme #1, the deformation of the scheme #2 of the other key points are smaller than that of the scheme #1 for the heterogeneous rock mass. This shows that the deformation of the tunnel is mainly controlled by the rock mass, and the heterogeneous weak interlayer affects only deformation. Furthermore, the better the rock mass, the greater the influence of the weak interlayer is.

Lateral pressure coefficient

The lateral pressure coefficient (Table 10) may also affect or even aggravate the influence of the heterogeneity of the rock mass on the tunnel stability. When the thickness is 1.0 m and the number of weak interlayers is 6, the deformation of the tunnel is shown in Fig. 7.

Figure 7 shows that the displacement of each key point of the tunnel increases with the increase in the lateral pressure

coefficient, and the displacement of the right-side wall increases significantly. Except for the left-side wall, HED of the other key points is greater than the equivalent HOD. When the weak interlayer is relatively far away from the tunnel, the influence of the lateral pressure coefficient on the displacement is weakened. Except for the right-side wall, HED of the other key points is less than the equivalent HOD. This shows that the lateral pressure coefficient will aggravate the influence of rock mass heterogeneity on the stability of tunnel surrounding rock mass.

Site distribution of weak interlayer

The location of the heterogeneous weak interlayer may also affect the stability of the surrounding rock mass, as shown in Fig. 1b and c. When the distance is 0 m, the thickness is 1.0 m, the number of weak interlayer is 6, and the same heterogeneous weak interlayer is distributed on the side wall or vault, the tunnel deformation is shown in Fig. 8. When the random rock mass is distributed on the vault, the deformation law of each key point is similar to that distributed on the side wall, which has the greatest influence on the vault. The deformation of the side wall when the weak interlayer distributes on the right-side wall, is greater than, the deformation of the vault when the weak wall distributes on the vault. This may be because of the arch effect and the stress
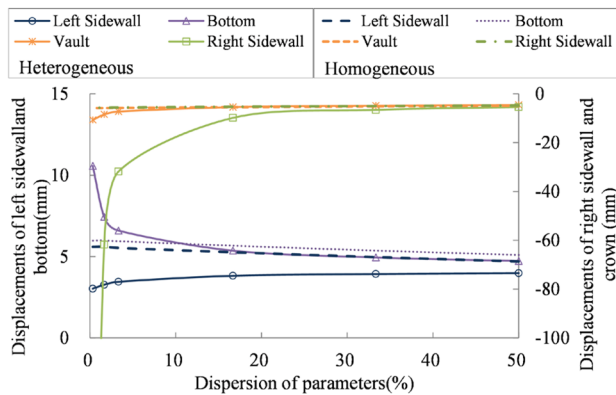
(a) Dispersion of parameters on weak interlayer
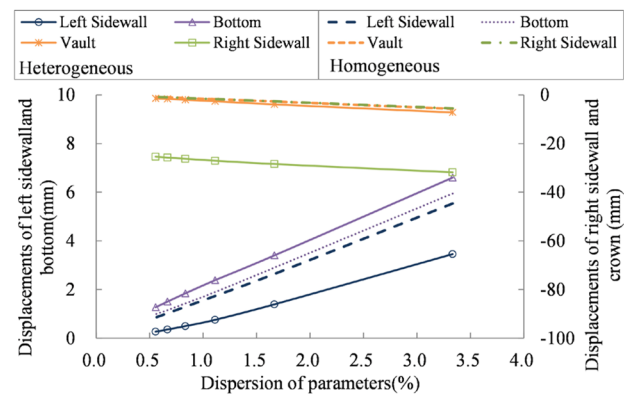
(b) Dispersion of parameters on rock mass

Fig. 6 The influence of dispersion of parameters on tunnel deformation

Table 10 Analysis scheme for the lateral pressure coefficient	Item	1	2	3	4	5	6	7
	Lateral pressure coefficient	0.25	0.50	0.75	1.00	1.25	1.50	1.75

field weakening the influence of the weak interlayer on the deformation of the tunnel.

In summary, the deformation of the tunnel is mainly affected by the adjacent weak interlayer and the main influence distance is about 0.5 D. The thickness and number of interlayers are dominant, when the interlayer has soft-hard and hard-soft distributions. The interlayer occupancy rate and HED increases with the increase in the number of interlayers. When the weak interlayer is randomly distributed, the deformation of the wall increases with the decrease in the average value of the parameters, and it is significantly affected by the standard deviation. Simultaneously, the lateral pressure coefficient of the surrounding rock mass and the degree of dispersion of the parameters aggravate the deformation of the tunnel of the heterogeneous rock mass. Therefore, the methods for evaluating the stability of the heterogeneous rock mass tunnel with weak interlayer distribution is worthy of further study.

Tunnel stability evaluation methods

The stability evaluation of surrounding rock has always a critical problem in underground cavern engineering. In practical engineering, evaluating the stability of heterogeneous tunnels generally use homogeneous stability evaluation methods (Ma et al. 2009). Commonly used stability evaluation methods for homogeneous tunnels mainly include the strength criterion (Gao et al. 2016), critical deformation (Li and Zhu 2013), catastrophe theory (Wang et al. 2019), and indirect evaluation methods (Li et al. 2014; Liu et al. 2015).

The following is a brief description on the modified Fenner formula evaluation method based on critical deformation.

Formula evaluation method of tunnel stability

The application of the strength criterion index method to engineering practice is difficult because of various factors, such as geological environment and construction conditions. Thus, the deformation index method is more commonly used. The surrounding rock mass is failure when the deformation or deformation rate of the tunnel exceeds a critical value. The judgment methods, such as plastic zone, cracking zone, damage zone, and stress and deformation fields, which are based on the current numerical analysis methods, have been gradually applied in design and construction. However, in-situ deformation monitoring is still one of the most convenient, reliable, and direct methods for evaluating surrounding rock mass stability, and it is also the mainstream method in engineering construction. Among these methods, the empirical formula method (Chen 2004), the national standard method (China metallurgical construction association 2015), the modified Fenner formula method (Li et al. 2006a, b), and that based on the safety of the support structure to evaluate the stability of the surrounding rock mass (Li et al. 2014; Liu et al. 2015), are relatively common operational methods. The empirical formula method mainly considers the influence of the tunnel span, tunnel height, and uniaxial saturated compressive strength of the surrounding rock mass. The specification method imposes severe restrictions on the tunnel span, surrounding rock type, and buried depth to ensure its applicability; however, the considerations
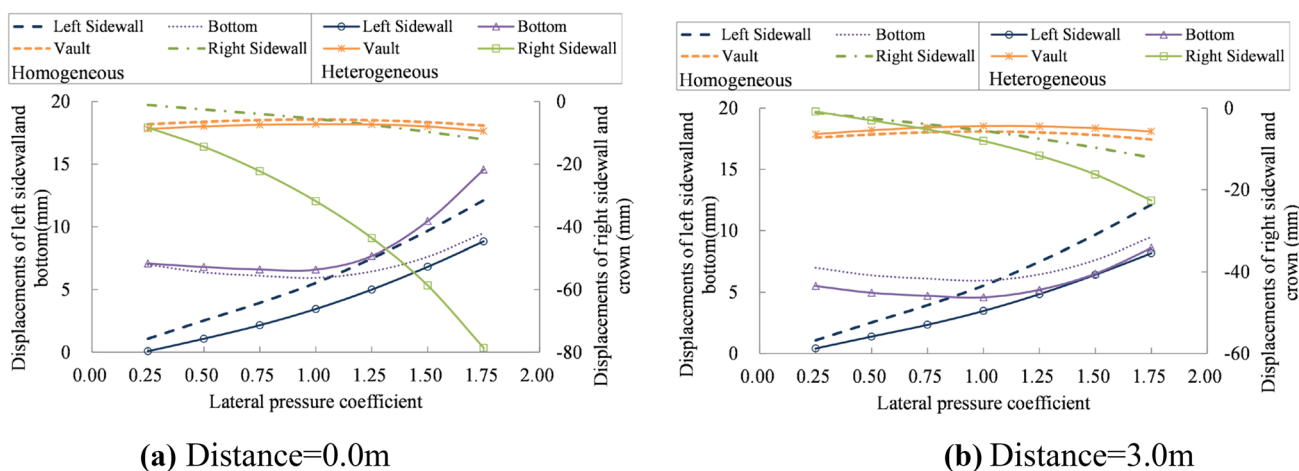

(a) Distance=0.0m

(b) Distance=3.0m

Fig. 7 The Influence of lateral pressure coefficient on tunnel deformation

(a) Weak interlayer distributes in right wall

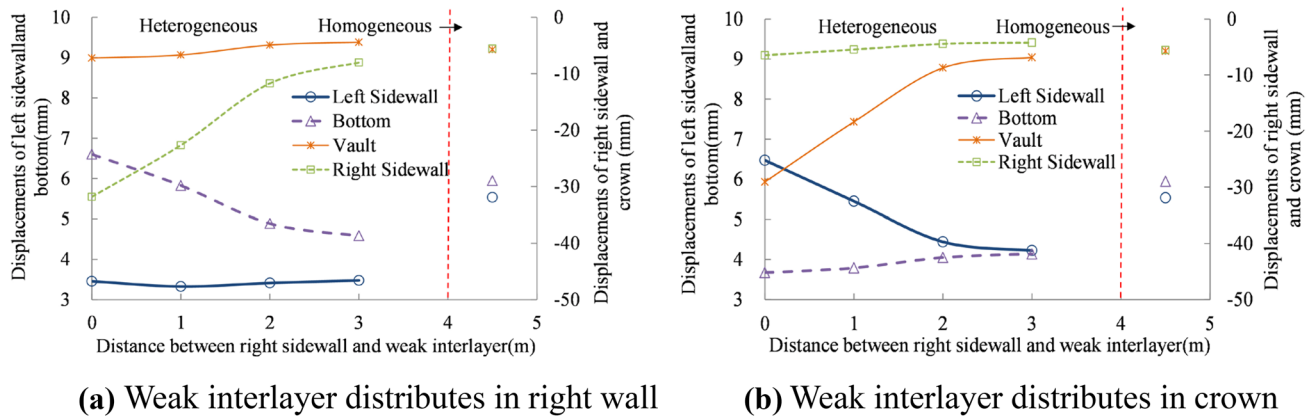

(b) Weak interlayer distributes in crown

Fig. 8 The influence of weak interlayer distribution on tunnel deformation

for lithology and depth are also based on experience and are relatively rough. There are no direct quantitative relationships among the deformation modulus (E), cohesion (c), internal friction angle (φ), and buried depth of the tunnel (H), thereby resulting in a wide range of allowable deformation and poor operability. Therefore, we proposed an evaluation method based on the modified Fenner formula from the elastic–plastic analytical solution of a circular tunnel.

For a circular tunnel, the plane strain condition is considered, and the static lateral pressure coefficient of the surrounding rock is 1.0. The elastoplastic analysis of the surrounding rock stress and deformation is as follows (Yu et al. 1983).

The equilibrium equation of circular tunnel is

$$\frac{\partial \sigma_r}{\partial r} + \frac{\sigma_r - \sigma_\theta}{r} = 0 \tag{1}$$

It satisfies the Mohr–Coulomb plasticity condition,

$$\frac{\sigma_r^P + C \cot \varphi}{\sigma_\theta^P + C \cot \varphi} = \frac{1 - \sin \varphi}{1 + \sin \varphi} \tag{2}$$

The plastic zone stress can be obtained by using (1) and (2) simultaneously as

$$\sigma_r^P = (P_i + C \cot \varphi)\left(\frac{r}{r_0}\right)^{\frac{2 \sin \varphi}{1 - \sin \varphi}} - C \cot \varphi$$

$$\sigma_\theta^P = (P_i + C \cot \varphi)\left(\frac{1 + \sin \varphi}{1 - \sin \varphi}\right)\left(\frac{r}{r_0}\right)^{\frac{2 \sin \varphi}{1 - \sin \varphi}} - C \cot \varphi \tag{3}$$

The stress coordination conditions are met at the elasto-plastic interface (or when the radius of the plastic zone is R_0),

$$\sigma_r^e = \sigma_r^P = \sigma_{R_0}, \quad \sigma_\theta^e = \sigma_\theta^P \tag{4}$$

For the elastoplastic interface,

$$\sigma_r^e + \sigma_\theta^e = 2P = \sigma_r^P + \sigma_\theta^P \tag{5}$$

When Formula (5) is incorporated into the plastic conditional Formula (2), the stress at the radius R_0 of the plastic zone is

$$\sigma_r = P(1 - \sin \varphi) - C \cos \varphi = \sigma_{R_0}$$

$$\sigma_\theta = P(1 + \sin \varphi) + C \cos \varphi = 2P - \sigma_{R_0} \tag{6}$$

The modified Fenner formula is obtained by bringing $r = R_0$ into the plastic zone stress (3) and considering (6) as

$$R_0 = r_0 \left[\frac{(C \cot \varphi + P)(1 - \sin \varphi)}{P_i + C \cot \varphi}\right]^{\frac{1 - \sin \varphi}{2 \sin \varphi}} \tag{7}$$

The elastic zone stress and displacement are

$$\sigma_r^e = P - (P \sin \varphi + C \cos \varphi)\frac{R_0^2}{r^2}$$

$$\sigma_\theta^e = P + (P \sin \varphi + C \cos \varphi)\frac{R_0^2}{r^2}$$

$$u_e = \frac{(P \sin \varphi + C \cos \varphi)R_0^2}{2Gr} \tag{8}$$

It is assumed that the volume of the plastic zone is constant under small deformation conditions, and the deformation coordination condition is based on the elastic–plastic interface.

$$u_e = u_P \tag{9}$$

The plastic zone displacement expression is obtained,

$$u_P = \frac{(P \sin \varphi + C \cos \varphi)R_0^2}{2Gr} \tag{10}$$

Further, the following form the subsequent steps:

(1) When the surrounding rock surface of the tunnel just reaches the shear plastic limit, or when the surrounding rock does not have the plastic zone, $R_0 = r_0$, the maximum deformation at the wall of the circular tunnel ($r = r_0$) is

$$u_P = \frac{(P \sin \varphi + C \cos \varphi) r_0^2}{2G r_0} = \frac{r_0 \sin \varphi}{2G}(P + C \cot \varphi) \quad (11)$$

(2) However, after the tunnel is excavated, there will always be a part of the surrounding rock entering into the plastic state. When the radius of the plastic zone is R_0 and $R_0 > r_0$, the displacement at the wall $r = r_0$ is

$$u_P = \frac{(P \sin \varphi + C \cos \varphi) R_0^2}{2G r_0} = \frac{R_0^2 \sin \varphi}{2G r_0}(P + C \cot \varphi) \quad (12)$$

(3) When the plastic zone appears, irrespective of the support resistance ($Pi = 0$) and considering the modified Fenner formula (7), the displacement at the wall $r = r_0$ is

$$u_P = \frac{\sin \varphi}{2G r_0}(P + C \cot \varphi) r_0^2 \left[\frac{(C \cot \varphi + P)(1 - \sin \varphi)}{C \cot \varphi} \right]^{\frac{1 - \sin \varphi}{\sin \varphi}}$$

$$= \frac{r_0 \sin \varphi}{2G}(P + C \cot \varphi) \left[\frac{(C \cot \varphi + P)(1 - \sin \varphi)}{C \cot \varphi} \right]^{\frac{1 - \sin \varphi}{\sin \varphi}} \quad (13)$$

(4) It is assumed that the volume of the plastic zone is not constant, and the shearing expand phenomenon is considered. When the radius of the plastic zone is R_0 and $R_0 > r_0$, the displacement at the wall $r = r_0$ is

$$u_P = \frac{2(P \sin \varphi + C \cos \varphi) R_0^2}{2G r_0}(1 - \mu) + \frac{r_0(1 - 2\mu)}{2G}(P + C \cot \varphi) \left[(1 - \sin \varphi) \left(\frac{r_0}{R_0} \right)^{\frac{2 \sin \varphi}{1 - \sin \varphi}} - 1 \right] \quad (14)$$

(5) When the lateral pressure coefficient, $\lambda \neq 1.0$, the displacement at the wall $r = r_0$ is (Zhang 2015)

$$u_p = \frac{1}{4G r_0} \left[R_0^2 + (1 - \lambda) R_0 f(\theta) \right] \bullet$$

$$\left\{ \sin \varphi[(1 + \lambda)P + 2C \cot \varphi] \left[1 + \frac{(1 - \lambda) \sin \varphi}{R_0(1 - \sin \varphi)} f(\theta) \right] - P(1 - \lambda) \cos 2\theta \right\} \quad (15)$$

The radius of the plastic zone is as follows:

$$R_0^* = R_0 + R_0 f(\theta) = R_0(1 + f(\theta)) \quad (16)$$

$$R_0 = r_0 \left\{ \frac{[(1 + \lambda)P + 2C \cot \varphi](1 - \sin \varphi)}{2C \cot \varphi} \right\}^{\frac{1 - \sin \varphi}{2 \sin \varphi}} \quad (17)$$

$$f(\theta) = \frac{(1 - \lambda)(1 - \sin \varphi)P}{\sin \varphi \, [(1 + \lambda)P + 2C \cot \varphi]} \cos 2\theta \quad (18)$$

When the radius (R_0^*) of the plastic zone is R_0 and $R_0 = R_0^*/(1 + f(\theta))$ in the displacement formula (16). For the side wall and the vault, the θ values are 0º and 90º, respectively. where λ is the lateral pressure coefficient, u_P is the vault settlement or side wall convergence value (m), $P = \gamma H$ is the stress of the surrounding rock mass (Pa), H is the buried depth of the tunnel (m), γ is the unit weight (N/m^3), r_0 is the tunnel radius (m), R_0 is the plastic zone radius (m), E is the deformation modes of the surrounding rock mass (Pa), μ is Poisson's ratio, C is the cohesion (Pa), φ is the internal friction angle (°), and G is the shear modulus of the surrounding rock mass (Pa). The plastic zone radius, R_0, can be considered initially according to the length L of the system bolt, i.e., $R_0 = L + r_0$. For non-circular tunnels, such as gate hole and horseshoe shape, when calculating the vault settlement deformation, the radius r_0 can be taken as a span; and when calculating the side wall convergence deformation, the radius r_0 can be taken as the height (Li et al. 2006a, b; Li et al. 2014).

Various factors, such as surrounding rock mass strength, depth and geometry of the tunnel, are considered explicitly and scientifically in the method that has greater reliability, operability, and applicability. This method not only has been applied and verified in the diversion tunnel of the Zipingpu hydraulic project, water intake tunnel of the Tianlonghu hydropower project, and diversion tunnel of the Wudu Diversion Project II (Chen et al. 2004), but also has been added into the fast analysis system for tunneling (FAST) (Li et al. 2015); and in the stability analysis and evaluation of the diversion tunnel of the Yellow River Jishixia hydropower station and the underground powerhouse of the Laxiwa hydropower station (Li et al. 2006a, b).

Application of the stability evaluation method

The method described in the previous section is based on homogeneous rock mass tunnels, and the surrounding rock

in actual engineering is mostly non-uniformly distributed. Therefore, each parameter of the surrounding rock mass in the analytic function should also be a variable and a function related to position. The elastoplastic solution of cohesion *C* as the plastic zone depth decreases linearly has been deduced. The results of comparing and analyzing a case show that the change in *C* value has a significant effect on the calculation result. The average *C* value of the plastic zone should be used in the calculation (Yu et al. 1983). The discrepancy in displacements, stresses, and plastic zones in the surrounding rock mass was analyzed for cases with different fault thickness and locations, as well as inner forces and stresses in the sprayed concrete lining system through the system numerical experiments (Zhang et al. 2017). To determine the influence of fault orientation on the surrounding rock mass stability of a mine roadway tunnel, scaled model studies of the strata movement were conducted (Hobbs 1968, 1969). The effects of faults on mining shafts stability were investigated by field investigation and numerical modeling (Bruneau et al. 2003a, b).

However, the actual surrounding rock mass may be a heterogeneous body containing multiple weak interlayers. When performing tunnel stability analysis and evaluation, the formula results derived from hypothesis simplification may not be applied directly. According to the actual situation of the heterogeneous distribution of the surrounding rock mass, the critical deformation should be adjusted accordingly (for example, multiplied by an expansion factor). For Scheme 1 of previous section (weak interlayer, the distance is 4 m, and the thickness of the plastic zone is 1.0 m), the critical deformation can be obtained by an analytical method, as presented in Table 11.

It can be seen from Table 11 that after the tunnel is excavated, some of the surrounding rock mass must enter the plastic state; thus, critical deformation obtained by the nonplastic zone method M1 is small. The thickness of the plastic zone of the equivalent homogeneous rock mass is about 1.0 m. Thus, the critical deformation is close to that of the equivalent homogeneous rock mass, when the radius of the plastic zone is 4.0 m for the method M2. The radius of the plastic zone obtained from the modified Fenner formula is

0.59–0.64 m; thus, its critical deformation is slightly smaller than that of the equivalent homogeneous rock mass. When considering shearing expand phenomenon, critical deformations are relatively larger. Therefore, when the lateral pressure coefficient is closer to 1.0, M2 and M4 are better for evaluating stability of homogeneous rock mass tunnels. For a heterogeneous rock mass tunnel, the critical deformation should be multiplied as an adjustment factor. When the interlayer appears on the side wall, the critical deformation of the vault should be reduced by 0–9% and 6%–15% for M2 and M4, respectively. When the interlayer appears on the vault, the opposite is true. The core of the stability evaluation process of the heterogeneous rock mass tunnels is to obtain the radius of the plastic zone and the distribution of weak interlayer. Further, if conditions permit, the heterogeneous distribution of the surrounding rock should be obtained as much as possible, and the heterogeneous calculation and analysis of the tunnel should be performed to obtain the plastic zone. When the distribution of surrounding rock is not available, the design length of the anchor may be approximated to replace the thickness of the plastic zone (Li et al. 2006a, b; Li et al. 2014). The following is a brief description of the method for conducting heterogeneous tunnel stability analysis and evaluation via the traffic tunnel of the *Sanhekou* hydro-junction project.

Case study

To obtain heterogeneous parameters and establish a heterogeneous model of the surrounding rock mass, we performed a field drilling process monitoring apparatus (DPMA) system (He et al. 2019a, b) test and geological exploration at the traffic tunnel of the *Sanhekou* hydro-junction project.

Project overview

The project of water diversion from Hanjiang River to Weihe River, as showed in Fig. 9, is located in the Qinling Mountains in the southern part of Shaanxi Province and is a large-scale water transfer project spanning from the Yellow River

Table 11 Limit displacements by analytical evaluation methods

Thickness (m)	Heterogeneous (mm)				Homogeneous (mm)				Evaluation methods (mm)			
	Vault	Left sidewall	Right sidewall	Bottom	Vault	Left sidewall	Right sidewall	Bottom	M1	M2	M3	M4
1	−4.38	3.79	−5.80	4.48	−4.40	4.24	−4.24	4.60	2.46	4.38	3.52	4.66
2	−4.43	3.66	−6.51	4.48	−4.62	4.44	−4.44	4.80	2.56	4.55	3.71	4.83
3	−4.44	3.57	−6.95	4.48	−4.85	4.64	−4.64	4.99	2.66	4.73	3.87	5.02
4	−4.45	3.50	−7.24	4.49	−5.13	4.89	−4.89	5.25	2.76	4.91	4.06	5.21

M1 indicates no plastic zone, M2 indicates plastic zone radius $R_0 = 4.0$ m, M3 indicates obtaining the plastic zone by the modified Fenner formula, and M4 indicates plastic zone radius $R_0 = 4.0$ m considering shearing expand phenomenon
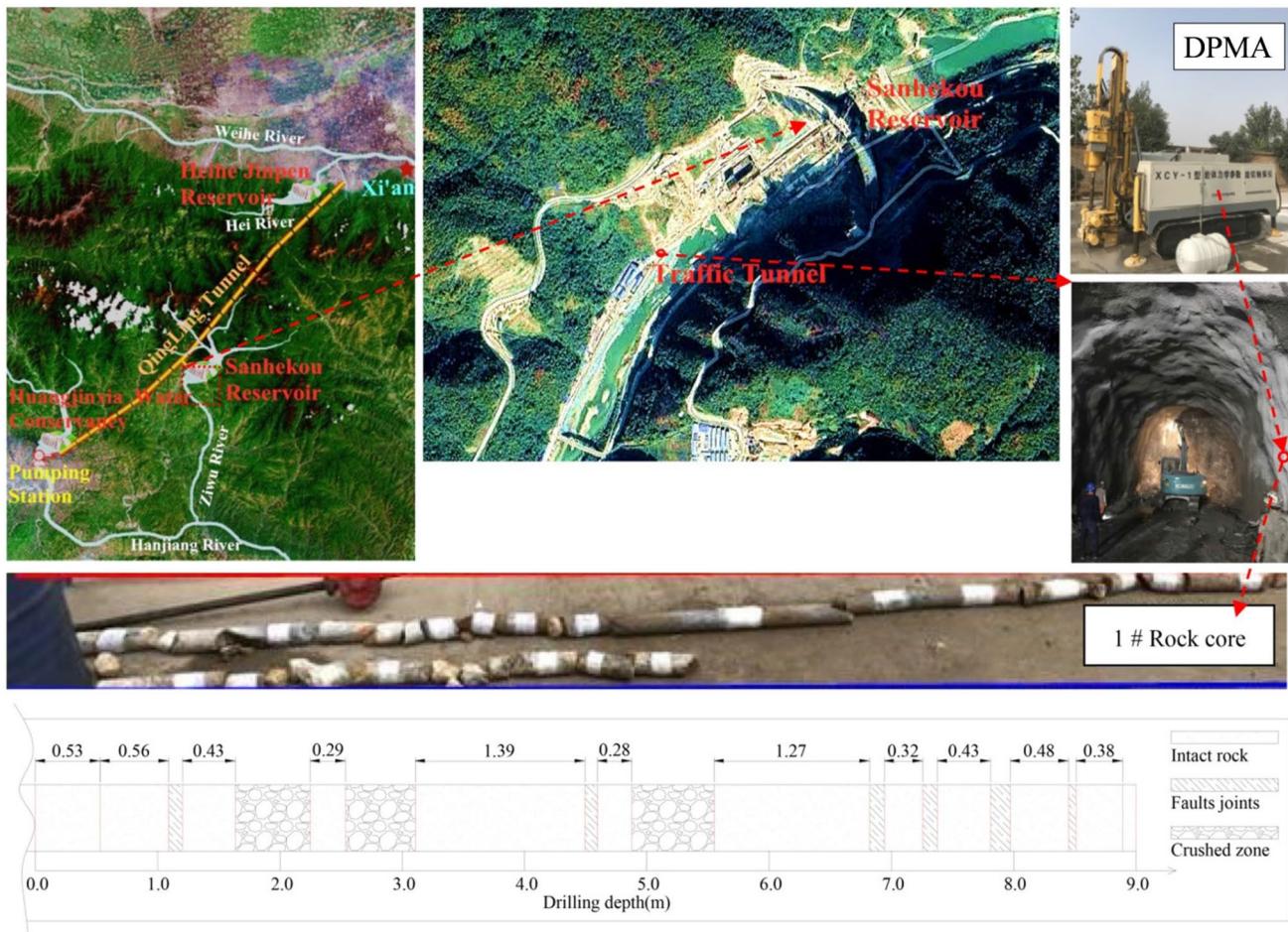
Fig. 9 Water diversion project from the *Hanjiang* River to *Weihe* River and the rock mass DPMA system test (He et al. 2019a, b)

to the Yangtze River. The engineering process is to transfer water from the *Hanjiang* River basin in southern Shaanxi to the *Weihe* River basin in the *Guanzhong* area. It consists of three parts; the *Huangjinxia* hydro-junction, *Sanhekou* hydro-junction, and *Qinling* water transmission tunnel.

Establishing heterogeneous tunnel model of rock mass

To meet the size requirements of the electromechanical equipment, a rectangular conduit with circular upper wall cross-section type tunnel is adopted. The primary information of the analyzed tunnel is presented in Table 12. To simplify the calculation, all supporting measures are not considered. In this section, we build and mesh the model, and calculate and verify the same by the FLAC^{3D} software, wherein only half of the tunnel model is used to simulate the excavation of the bore hole, as shown in Fig. 10.

In Fig. 10, the drilling hole is drilled horizontally inward to approximately 9 m in the right-side wall, to consider the model heterogeneity, based on the rock core distribution. On the basis of parameter heterogeneity segmentation, the

surrounding rock mass of the model's right wall, which is equal to the drilling depth of the rotary cutting system test, is also segmented by 1 m to approximate the change in the actual surrounding rock mass. When the element thickness is 1 m and the element size is 0.2–0.5 m, the total number of nodes after meshing is 24,522, and the number of elements is 16000.

Acquiring heterogeneous parameters of rock mass

The project area is mainly composed of metamorphic sandstone and crystalline limestone of the Lower Silurian Meiziya Formation. It is partially interspersed with marble and Indosinian intrusive pegmatite and quartz veins. The geological exploration and laboratory test data (Guo et al. 2014a, b) show that the traffic tunnel is mainly around II and III class of surrounding rock mass, the mechanical parameters of the rock mass are summarized in Table 13.

To obtain the heterogeneous parameters of the surrounding rock mass, the DPMA (He et al. 2019a) system is used at the traffic tunnel of the *Sanhekou* hydro-junction project as shown in Fig. 9. The heterogeneous rock core distribution

Table 12 Primary information of the analyzed tunnel

Item	Description
Cross-section	Rectangular conduit with circular upper wall
Height	$h = 5.56$ m
Span	$b = 5.00$ m $= D$
Angle of the top arch	$\beta = 148.12°$
Overburden	$H = 100.0$ m
Lateral pressure coefficient	$\lambda = 0.3$
Model size	$\triangle X = 22.5$ m, $\triangle Z = 45.0$ m, $\triangle Y = 1.0$ m
Boundary condition	Top, $Z = 45.0$ Apply $P1 = -(H+h-30) \rho g$
	Bottom, $Z = 0.0$ Fix-Z Apply $P2 = -(H+h+15) \rho g$
	Plane $X = 0.0$, $X = 22.5$ Fix-X Apply $P3 = (P2 + \rho g \cdot Z) \lambda$
	Plane $Y = 0.0$, $Y = 1.0$ Fix-Y Apply $P4 = P3$

characteristics of the tunnel surrounding rock mass with drilling length is presented. The rotary cutting test drilled in a total of 9 m, and there are large fluctuations in the drilling parameters in the 2-3-m and 5-6-m sections, thereby indicating that the two subsections of the surrounding rock mass may be a fault or relatively fractured. While the other sections are relatively stable and only produce small fluctuations locally, which shows that the surrounding rock mass is relatively complete and only small cracks exist locally.

Currently, many researchers have proposed various empirical relations for estimating the deformation modulus of rock mass based on rock quality designation, rock mass rating, Q-system, and geological strength index (GSI) (Bertuzzia et al. 2016; Bieniawski 1973; Barton 2002; Hoek and Brown 1980). However, empirical approaches may exhibit a great variation when compared to each other. For the same rock sample, different rock mass parameters may be obtained using different methods (He et al. 2019a, b, 2020, 2021a, b).

The rotary cutting parameters were obtained by the field DPMA system test. After segmenting by 1 m for 1# rock core, the heterogeneous deformation modulus of the surrounding rock mass was transformed by the above-mentioned empirical relations. Further, the 16 group parameters were averaged and arranged in the descending order, and were classified according to the surrounding rock mass classification standard. The minimum values and standard deviations of each group of parameters are also analyzed, as presented in Table 14.

It can be seen from Table 14 that the parameters that change rules of each group are basically the same. Furthermore, the minimum values appear in the 2-3-m and 5-6-m segments,

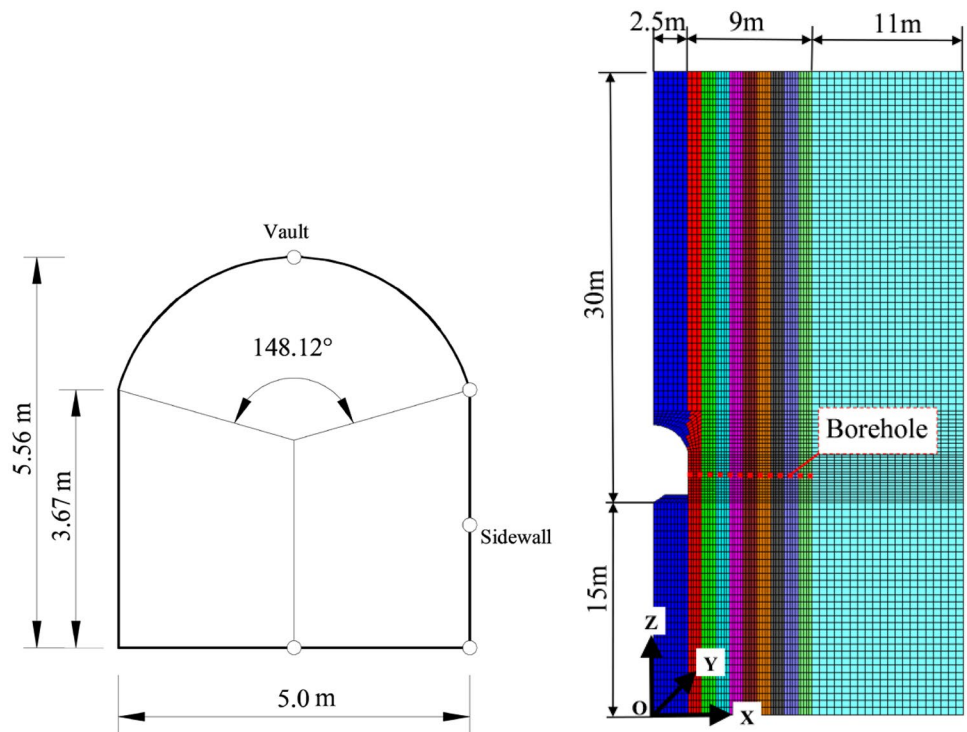**Fig. 10** Tunnel model of the heterogeneous rock mass

Table 13 Mechanical parameters of the rock mass

Material	Density, ρ (kg/m^3)	Deformation modulus, E (GPa)	Poisson ratio, μ	Cohesion, c (MPa)	Frictional angle, φ (°)
Rock mass	2750	17.91	0.25	1.15	49

thereby indicating that the calculated parameters of each method can reflect the geological characteristics of the original rock mass; however, there is only quality difference in the whole rock mass. The deformation modulus range of the rock mass calculated using different methods are also relatively large, ranging from 0.9 to 64.4 GPa, with an average value of 18.9 GPa, which is close to the weighted average of the geological survey (GS). The average value of each group is between 5.2–55.0 GPa and appears from class I–IV surrounding rock mass. However, the GS shows that the traffic hole is mainly class II and III surrounding rock mass. Thus, the parameters obtained from the calculation methods (1, 2, 5) may be larger, and the parameters obtained by the calculation methods (11, 15) may be smaller. The minimum value controlled by the 5–6 m rock core segment and the performed fluctuation in the average value and the standard deviations of each group are also similar. The dispersion degree of the parameters obtained by the second calculation method is the largest, while that by the eleventh calculation method is the smallest. The average value of the calculated parameters of the sixth and seventh groups are close to the average value of the GS. However, it may not be sufficient to reflect the traits of the original rock mass because of the influence of the parameter's dispersion degree.

Stability analysis and evaluation of the heterogeneous rock mass tunnel

Comparative analysis for various empirical relations of rock mass deformation modulus

According to the basic physical and mechanical parameters of the surrounding rock mass and the 16 group deformation modulus from different empirical relations ordered above are used for analysis. The Mohr–Coulomb model is adopted when performing elastic–plastic analysis, using the numerical model described above. The homogeneous analysis (HA), wherein the deformation modulus of the whole model area is the average value of each segment, and the divided heterogeneous analysis (DHA), wherein the deformation modulus of each segment is the value of 1 m in the drilling depth and the remaining regions are the adjacent segment parameters, were executed as well. The results of the GS can also be presented. The deformation on HA and DHA on the vault and the side wall obtained under elastic–plastic conditions are shown in Fig. 11.

Figure 11 shows that the deformation of the vault and side wall increases with the decrease in the average deformation modulus. The DHA deformation is smaller than the HA deformation at the vault; however, the DHA deformation is slightly larger than the HA deformation at the side wall. Furthermore, the smaller the deformation modulus, the greater the deformation difference between DHA and HA. Under elastic–plastic conditions, the deformations of the GS parameters are close to those of No. 5 and No. 6, and are smaller than those of the most group parameters. The HA deformation of the vault is 4.9 times that of the side wall, which is similar to the GS; however, the DHA deformation of the vault is 4.3 times that of the side wall. The deformation of the side walls for HA and DHA are quite different under the elastic–plastic conditions, which may be mainly affected by the minimum value and standard deviations of the group parameter. That is the standard deviation increase proportionally with the decrease in the minimum value, and the difference in the deformation between HA and DHA becomes more obvious. When the Drucker-Prager model and the rock mass deformation modulus closed to the No. 10 (about 9.0 GPa) are adopted, the deformation on the vault and side walls are 4.7 and 2.8 mm, respectively, under no supporting conditions for *Qinling* tunnel of class III surrounding rock (Ren 2017). The deformations on the vault and side walls are 3.5 and 0.6 mm, respectively, under the elastic conditions for HA on No. 10. However, these are 3.8 and 0.8 mm, respectively, under the elastic–plastic conditions. The deformation is within the range required by the code, which is less than the result of Fenner formula. In other words, the tunnel meets the requirement of stability.

For HA and DHA, under elastic–plastic conditions for parameter No. 12, the distribution of displacement and plastic zone are shown in Fig. 12, and the critical deformation can be obtained by the analytical method presented in Table 15.

Figure 12 and Table 14 highlight that the overall distribution of the displacement is similar for HA and DHA, just the displacement of vault for HA is larger than that for DHA. The overall distribution of the plastic zone is similar for HA and DHA. However, the plastic zone of the DHA increases by 0.2 m on the side wall as compared with that of the HA. Meanwhile, the tensile plastic zone of the arch bottom and the arch foot reduces, and the shear plastic zone of the arch shoulder and the arch foot increases. The lateral pressure coefficient is 0.3; thus, methods M2 and M4 will no longer be applicable. At this time, the surrounding rock mass mainly produces vertical deformation on the vault and the bottom, while the horizontal deformation on the side wall is relatively smaller. The weak interlayer is distributed outside the right-side wall; thus, a part of the vertical pressure is unloaded. The displacement of the side wall and vault increases and decreases, respectively, as compared to the

Table 14 Deformation modulus (E) of the rock mass (GPa)

Methods	Numbering	Rock core subsection (m)									Average value			Minimum value	Standard deviation
		1	2	3	4	5	6	7	8	9	Value	Order 5~6	Rock grad		
Geological survey	0										17.91		III		
Bieniawski et al. (1978)	1	63.8	49.0	52.5	59.3	55.9	31.4	63.2	55.1	64.4	55.0	1	I	31.4	9.7
Serafim et al. (1983)	2	62.7	41.0	45.3	55.1	49.9	24.7	61.7	48.9	63.9	50.4	2	I	24.7	11.8
Read et al. (1999)	5	54.9	41.3	44.3	50.5	47.3	28.4	54.4	46.7	55.6	47.1	3	I	28.4	8.1
Gokceoglu et al. (2003)	9	35.7	20.4	23.3	30.1	26.4	10.5	34.9	25.7	36.6	27.1	4	II	10.5	8.0
Barton (2002)	6	23.1	17.7	19.0	21.5	20.2	11.4	22.9	19.9	23.3	19.9	5	III	11.4	3.5
Barton (2002)	7	18.4	15.6	16.2	17.5	16.9	12.9	18.3	16.7	18.6	16.8	6	III	12.9	1.7
Hoek et al. (1998)	12	18.8	14.1	15.1	17.2	16.1	10.1	18.6	15.9	19.0	16.1	7	III	10.1	2.7
Mitri et al. (1994)	4	12.7	11.7	12.0	12.4	12.2	10.2	12.7	12.1	12.7	12.1	8	III	10.2	0.8
Sonmez et al. (2006)	14	12.7	11.6	11.9	12.4	12.1	9.7	12.7	12.1	12.7	12.0	9	III	9.7	0.9
Hoek et al. (2002)	8	9.2	7.1	7.6	8.5	8.0	5.3	9.1	7.9	9.3	8.0	10	III	5.3	1.2
Gokceoglu et al. (2003)	10	9.0	6.7	7.2	8.3	7.7	4.8	8.9	7.6	9.1	7.7	11	III	4.8	1.3
Aydan et al. (2014)	16	11.0	4.6	5.6	6.9	5.9	2.2	10.0	9.1	10.9	7.4	12	III	2.2	2.9
Hoek et al. (2006)	13	7.6	5.1	5.6	6.8	6.2	3.2	7.5	6.1	7.8	6.2	13	III	3.2	1.4
Nicholson et al. (1990)	3	7.1	5.4	5.8	6.5	6.1	3.9	7.0	6.0	7.2	6.1	14	III	3.9	1.0
Sonmez et al. (2004)	11	6.1	5.5	5.6	5.9	5.7	4.9	6.0	5.7	6.1	5.7	15	IV	4.9	0.4
Zhang et al. (2004)	15	8.8	2.5	3.4	4.5	3.6	0.9	7.7	6.7	8.7	5.2	16	IV	0.9	2.7

Fig. 11 Deformation change curve with the average value of deformation modulus and its order
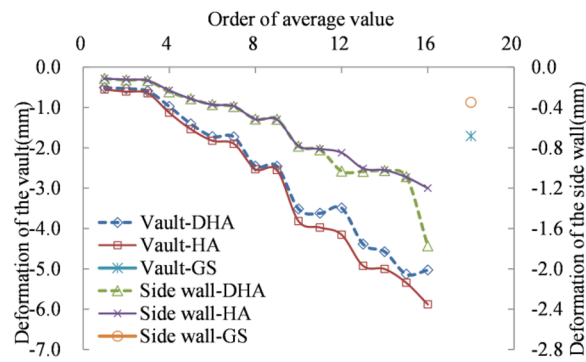
(a) Deformation with the order of the average value of deformation modulus
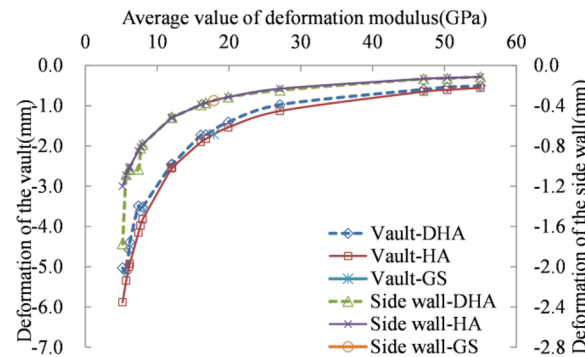
(b) Deformation with the average value of deformation modulus

equivalent homogeneous rock mass tunnel. The plastic zone calculated by the method M5-1 is smaller than the actual one. When the actual plastic zone is used for M5-2, the deformation on the vault and side wall is 4.06 and 0.76 mm, respectively. It is very close to the deformation of an equivalent homogeneous rock mass tunnel. Therefore, it is appropriate to evaluate the heterogeneous rock mass tunnel by reducing the vault deformation by 15%.

Difference in behavior between heterogeneity and homogeneity

From the above analysis, it can be seen that the homogeneous and heterogeneous parameters and models have a certain difference in terms of deformation, which has a considerable influence on the stability evaluation of the tunnel. Therefore, the designed test scheme is presented in Table 16, and the problem is briefly discussed. For simplicity, the No. 12 group surrounding rock parameters is still used. The deformation on the tunnel vaults and side walls, on different tunnel spans, ratio of height to span, and tunnel depth, are shown in Fig. 13, and the average change rate of deformation on vaults and side walls are presented in Table 17.

Figure 13 shows that the deformation of the vault and side wall increases with the increase in the tunnel span. HED is less than HOD for the vault. However, for the side wall,

there is a critical value of the tunnel span, 4.5 m. When the tunnel span is greater than 4.5 m, HOD is smaller than HED; however, when the tunnel span is less than 4.5 m, HOD is larger. The deformation difference increases with the increase in the span. The deformation on the vault and side wall increases with the increase in the ratio. HED is less than HOD for the vault. However, for the side wall, there is a critical value of the ratio, 1.05. When the ratio is greater than 1.05, HOD is smaller than HED; however, when the ratio is less than 1.05, HOD is larger. The deformation difference increases with the increase in the ratio. The deformation of the vault and side wall increases with the increase in the tunnel depth. HED is less than HOD for the vault. However, for the side wall, HED is larger than HOD. The deformation difference increases with the increase in the tunnel depth. Under most circumstances, the deformation of the side wall is smaller than the vault because of the participation of the fault fracture zone on the side wall. The larger the tunnel span (greater than 4.5 m) is, the higher the ratio of height to span is (greater than 1.05), and the greater the tunnel depth is; the side wall and the arch foot should be considered.

Verifying adjustment coefficient

The above analysis shows that irrespective of the parameter empirical relations, there are differences in the deformation
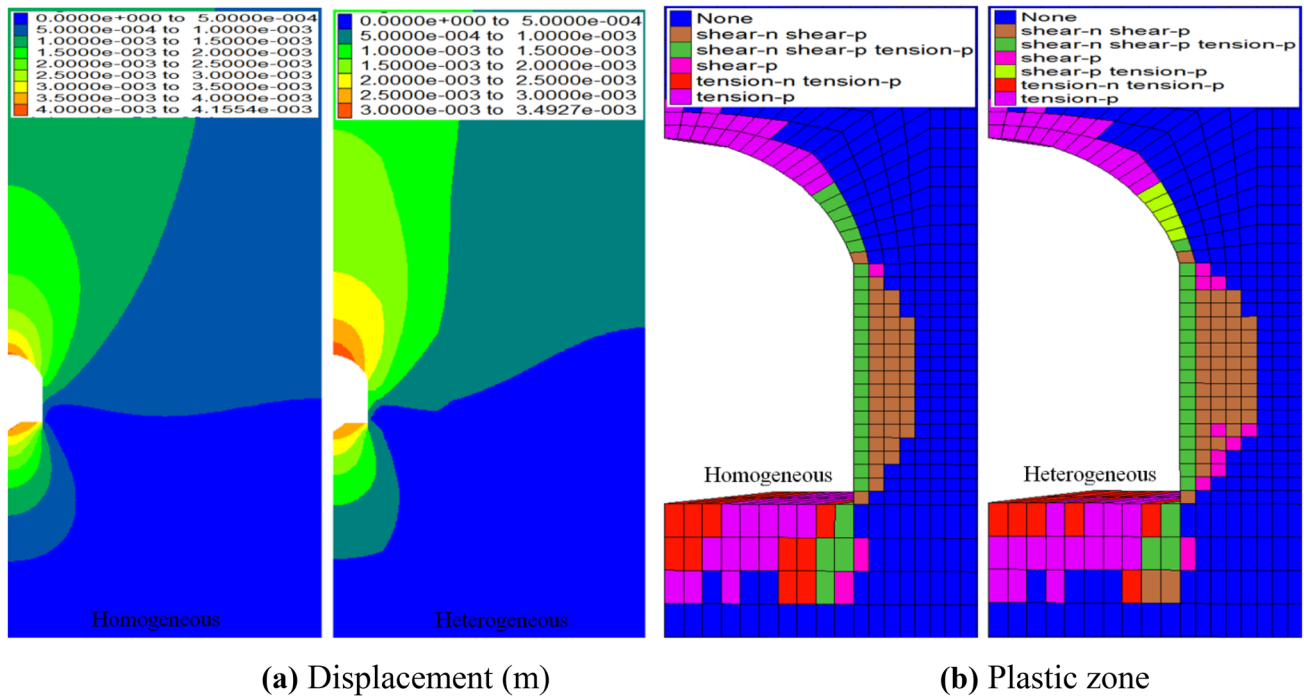
(a) Displacement (m)   **(b)** Plastic zone

Fig. 12 Distribution of displacement and plastic zone

of the key points of the tunnel with the homogeneous and heterogeneous parameter and models. Furthermore, when heterogeneity appears on the side wall, under different spans, ratio of height to span, depth of the tunnel, the difference degree on the deformation are different. Considering the heterogeneity of different positions or the heterogeneity of different depths, the difference degree is also different. If the stability evaluation of the tunnel is considered to be homogeneous, then it needs to be modified. Therefore, under elastic–plastic conditions for parameter No. 12, the influence degree of each factors on the tunnel stability evaluation are discussed. The deformation difference rate of the heterogeneous parameter and model of each factor relative to the homogeneous parameter and model are presented in Table 18.

Table 18 highlights that under different tunnel span, the deformation difference rates of vault are around − 15%, i.e., the critical deformation value of the vault for the evaluation method should be reduced by at least 15%. When the tunnel span is less than 5 m, the deformation difference rate of the side wall is negative. However, when the tunnel span is more than 5 m, the deformation difference rate of the side wall is positive and increases with the increase in the tunnel span. When the tunnel span is 3 m, the rate is − 17.06%, i.e., the critical deformation value of the side wall should be reduced by about 17%. For different ratios of height to span, the deformation difference rates of vault are around − 14% for EPA, i.e., the critical deformation value of the vault for each

evaluation method should be reduced by at least 14%. When the ratio of height to span is less than 1.1, the deformation difference rate of side wall is negative. However, when the ratio of height to span is more than 1.1, the deformation difference rate of the side wall is positive and increases with the increase in the ratio of height to span. Further, the increased range is gradually reduced. When the ratio is 0.8, the rate is − 36.63%, i.e., the critical deformation value of the side wall should be reduced by about 37%. For different tunnel depths, the deformation difference rates of the vault reduce with the increase in tunnel depth, and the rates are larger than − 15% when the tunnel depth is less than 200 m, i.e., the critical deformation value of the vault for each evaluation method should be reduced by at least 15%. The deformation difference rate of the side wall is positive, about 2.6% for EA, and the change is not obvious with the increase in the depth. However, the deformation difference rate of the side wall increases with the increase in tunnel depth.

In summary, when evaluating the heterogeneous tunnel by the homogeneous tunnel stability evaluation method, the critical deformation is too large in most cases. Thus, the stability assessment of deformation monitoring in an actual engineering project, the critical deformation value should be reduced according to the specific circumstances. If the distribution characteristics of the weak interlayer are not determined, it may be appropriately reduced by 15%.

Table 15 Limit displacements by analytical evaluation methods

Heterogeneous(mm)			Homogeneous(mm)			M5-1 (mm)			M5-2 (mm)		
Vault	Right sidewall	Bottom	Vault	Right sidewall	Bottom	Vault $R_0=2.78$ m	Right sidewall $R_0=2.9$ m	Bottom $R_0=2.78$ m	Vault $R_0=4.28$ m	Right sidewall $R_0=3.3/3.5$ m	Bottom $R_0=4.28$ m
−3.49	−1.03	2.96	−4.16	−0.85	4.01	1.17	0.60	1.17	4.06	0.76/0.85	4.06

Table 16 Experimental scheme

Parameters	Basic scheme	Comparison scheme
Tunnel span/m	5	3, 4, 6, 7, 8
Ratio of height to span	1.1	0.8, 0.9, 1.0, 1.2, 1.3
Tunnel depth/m	200	50, 100, 150, 250, 300

Discussion and application

It is an undeniable fact that the heterogeneity of the rock mass should be considered in the general engineering design and construction under the precondition of detailed and accurate geological exploration. The heterogeneity of the model and the parameters are particularly remarkable. Estimating the parameters of rock mass using empirical relations is different, because each method has its own applicability and superiority. After carefully and accurately investigating and analyzing the engineering rock mass, experienced geological engineers or experts proposed a qualitative description and reasonable suggestions as the boundary conditions of the parameter values were obtained from various methods. For simplicity, the 16th group parameters obtained from empirical relation by Aydan et al. (2014) was a good attempt. The deformation modulus of the surrounding rock mass was discussed only in the case study; however, it was sufficient to illustrate the surrounding rock heterogeneity. Moreover, the heterogeneity behavior of other parameters, such as cohesion, friction angle, and compressive strength, may be studied by imitating on the train of thought from the deformation modulus (He et al. 2019a, b).

The heterogeneity of a model is simulated by dividing the rock mass into continuous subsections and assigning different parameters to a segmented continuum. Comparing the characteristics of deformation or stress between the continuous subsections and the interface element to simulate faults or fracture zones (Zhang et al. 2017) need be studied further. In other words, the applicability of the two methods should be discussed. The divided heterogeneous model considers the whole rock mass as a continuum, which only reflects the heterogeneity of the surrounding rock mass through the parameters of each zone. The structural plane model separates the model only at the fault; thus, the whole rock mass is considered to be a discontinuous body. However, the rock mass outside the structural plane is still considered in terms of homogeneity. Thus, both methods can be used in the project, depending on the degree of development of the fault fissure and the influence degree of the fault fissure for the stability of the tunnel surrounding rock mass.

For the heterogeneous rock mass or non-circular tunnel, the evaluating method of tunnel stability based on the Fenner formula should be improved. In this study, we focus mainly on the impacts of various influencing factors to the deformation stability
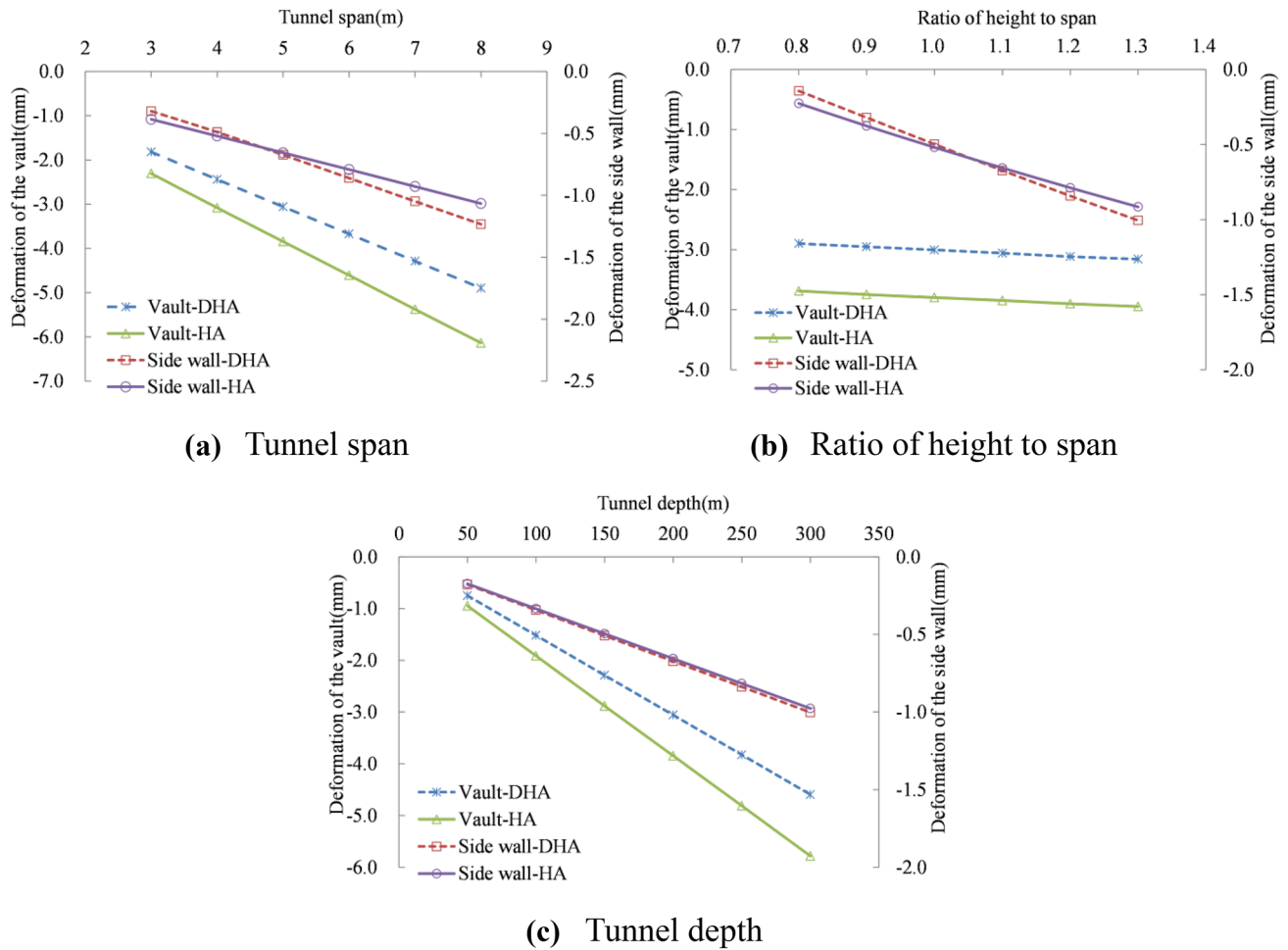
(a) Tunnel span

(b) Ratio of height to span

(c) Tunnel depth

Fig. 13 Deformation of key parts under different schemes

evaluation when the heterogeneous location is distributed on the side wall. When evaluating a heterogeneous tunnel using a homogeneous tunnel stability evaluation method, the critical deformation value should be reduced according to the specific circumstances or reduced by 15% (see the "Stability analysis and evaluation of the heterogeneous rock mass tunnel" section).

We conducted a 2-year safety monitoring work at the 2# diversion tunnel of the *Zipingpu* hydraulic project located in the Sichuan province, south-west of China. The tunnel passes through the F3 weak fracture zone. The rock mass of the zone is cracked and compacted. It is mainly fine particle with weak permeability and low shear strength. Its strength

Table 17 Average change rate of deformation

Influence parameters			Increment on tunnel span (/1 m)	Increment on ratio of height to span (/0.1)	Increment on tunnel depth (/1 m)
Increment of deformation (mm)	Vault	DHA	0.616	0.052	0.015
		HA	0.766	0.052	0.019
		Difference	0.863	0.789	0.014
	Side wall	DHA	0.183	0.172	0.003
		HA	0.136	0.138	0.003
		Difference	0.093	0.054	0.0003

The average change rate refers to the corresponding change of stress and deformation, when influencing factors averagely increase 1 m for the tunnel span and the tunnel depth or 0.1 for the ratio of height to span and the lateral pressure coefficient. The difference refers to the stress difference or deformation difference between HA and DHA

Table 18 Deformation difference rate (%)

Tunnel span/m		3	4	5	6	7	8
Deformation	Side wall	− 16.54	− 1.05	21.49	32.83	31.91	27.34
	Vault	− 19.02	− 17.92	− 15.95	− 15.29	− 15.45	− 15.78
Ratio of height to span		0.8	0.9	1.0	1.1	1.2	1.3
Deformation	Side wall	− 14.86	− 3.71	9.21	21.49	27.68	29.11
	Vault	− 19.07	− 18.42	− 17.47	− 15.95	− 15.09	− 14.40
Tunnel depth/m		50	100	150	200	250	300
Deformation	Side wall	3.06	3.12	10.38	21.49	24.86	22.63
	Vault	− 21.09	− 20.92	− 19.27	− 15.95	− 14.10	− 12.87

Deformation difference rate is the deformation difference on heterogeneous deformation and homogeneous deformation divide the deformation of homogeneous parameter and model

decreases rapidly after encountering water. It belongs to Class V surrounding rock, so the tunnel stability condition is very poor. According to the survey report, the deformation modulus of the surrounding rock is 0.3 GPa, the Poisson's ratio is 0.35, the Cohesion is 5 kPa, the friction angle is 20°, and the bulk density is 23 kN/m^3. As shown in Fig. 14, the drilling and blasting method adopts upper and lower bench excavation, and the lower bench is excavated in two steps. The initial support adopts pipe shed advanced grouting, steel arch grid and mold concrete support. According to the excavation mode, the 7-points convergence monitoring scheme is designed to timely obtain the deformation evolution process of surrounding rock after each step excavation of the tunnel.

On August 20, the Sect. 0+687.0~0+690.0 of the F3 weak fracture zone collapsed due to rainfall, untimely initial support and other reasons. And the collapse has a trend of further development, leading to the failure of rescue construction in a timely manner. Under the combined traction of the collapse, the collapse developed to the 0+680 section on August 22. The monitoring data of the adjacent 0+674.0 section is shown in Fig. 15. The tunnel section depth is about 100 m, the excavation radius is about 7 m and the plastic zone is 5 m. The maximum deformation values are 88.0~96.0 mm for the standard and empirical methods (Chen 2004; China metallurgical construction association 2015). However, the maximum allowable deformation of the surrounding rock is 73 mm according to the formula evaluation method of tunnel stability. Based on the above research results on the deformation difference between the homogeneous and heterogeneous surrounding rock on the tunnel, the critical deformation should be reduced by 15%, so the control deformation should be 62.1 mm. On August 22, the settlement of the vault has begun to increase, and the deformation is 61.9 mm. On August 23, the deformation increased significantly, and the surrounding rock may be unstable. The settlement of the section vault was 77.9 mm, which is less than the normative limit but exceeded the formula limitation and the heterogeneous results. So the monitoring team timely raised an emergency early warning. After the emergency reinforcement measures were taken on August 25–26, the deformation of the tunnel gradually became stable. Thus, field experts believed that a collapse was successfully avoided.
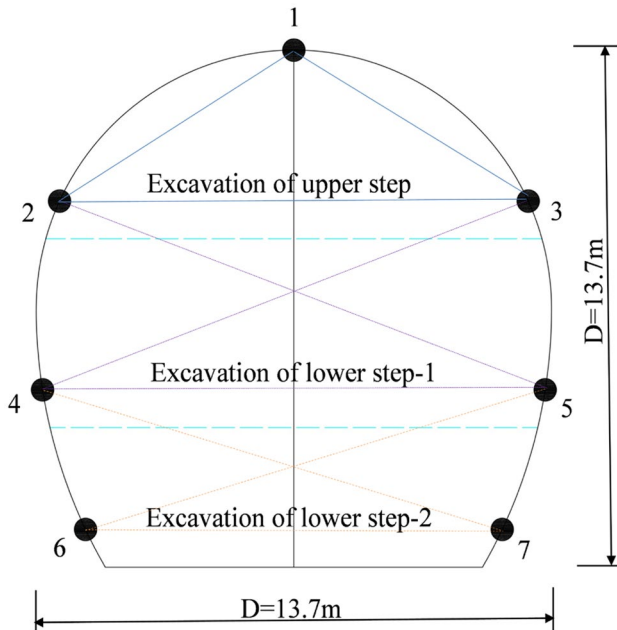

Fig. 14 Excavation mode and monitoring scheme of the 0+674.0 section at the 2# diversion tunnel
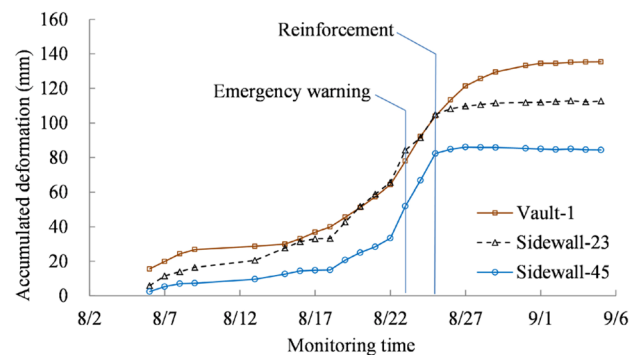

Fig. 15 Displacement monitoring curve of the 0+674.0 section

Conclusion

In this paper, we studied the influence of heterogeneity factors of the rock mass on the displacement of a tunnel based on the ideal heterogeneous rock mass tunnel model. We proposed a stability evaluation method of heterogeneous tunnel based on the elastoplastic analytical solution of a circular tunnel. We considered the traffic tunnel of the *Sanhekou* hydro-junction as an example and described how to obtain the heterogeneous parameters, establish a heterogeneous model, and analyze and evaluate the stability of the heterogeneous tunnel. The main conclusions are as follows:

(1) The deformation of the tunnel wall is mainly affected by the weak interlayer distributed adjacent to it. Under a weak interlayer, when the distance is constant, the deformation of the heterogeneous rock tunnel increases with the increase in the interlayer thickness. When the interlayer thickness is constant, HED increases with the increase in distance; the main influence distance is about 0.5 D. HED increases proportionally with the increase in the number of interlayers.

(2) When the interlayer occupancy rate and the number of interlayer are constant, the deformation caused by the soft-hard distribution is larger than that of the hard-soft distribution. The thickness and number of the interlayer are the dominant factors when the interlayer has soft-hard and hard-soft distributions, respectively. When the weak interlayer is randomly distributed, the deformation of the wall of the heterogeneous rock mass increases with the decrease in the average value of the parameters, and it is significantly affected by the standard deviation of the parameters.

(3) The core of the stability evaluation process of the heterogeneous rock mass tunnel is to obtain the radius of the plastic zone and the distribution of weak interlayer. If conditions permit, the heterogeneous distribution of the surrounding rock should be understood as much as possible, and the heterogeneity calculation analysis of the tunnel should be performed. If the surrounding rock distribution is not estimated, the design length of the bolt may be approximated to replace the thickness of the plastic zone.

(4) More fractures, poor quality of the surrounding rock mass, and significant heterogeneity will result in the obvious difference in the results of heterogeneous analysis and homogeneous analysis. If the distribution characteristics of the interlayer are not determined, they may be appropriately reduced by 15% to evaluate the tunnel stability of the heterogeneous rock mass. We verified the reliability of the stability evaluation method by monitoring the 2# diversion tunnel of the *Zipingpu* hydraulic project.

Declarations

References

Abdul MN, Muhammad ZE, Hafeezur R, Hankyu Y (2019) Geological and geomechanical heterogeneity in deep hydropower tunnels: a rock burst failure case study. Tunn Undergr Space Technol 84:507–521

Ado MR, Greaves M, Rigby SP (2019) Numerical simulation of the impact of geological heterogeneity on performance and safety of THAI heavy oil production process. J Petrol Sci Eng 173:1130–1148

Aydan Ö, Ulusay R, Tokashiki N (2014) A new rock mass quality rating system: rock Mass Quality Rating (RMQR) and its application to the estimation of geomechanical characteristics of rock masses. Rock Mech Rock Eng 47:1255–1276

Barton N (2002) Some new Q-value correlations to assist site characteristics and tunnel design. Int J Rock Mech Min Sci 39:185–216

Bieniawski ZT (1978) Determining rock mass deformability: experience from case histories. Int J Rock Mech Min Sci 15(5):237–247

Bruneau G, Tylerb DB, Hadjigeorgiou J, Potvin Y (2003a) Influence of faulting on a mine shaft a case study: part I-Background and instrumentation. Int J Rock Mech Min Sci 40:95–111

Bruneau G, Tylerb DB, Hadjigeorgiou J, Potvin Y (2003b) Influence of faulting on a mine shaft a case study: part II-Numerical modelling. Int J Rock Mech Min Sci 40:113–125

Bertuzzia R, Douglas K, Mostyn G (2016) Improving the GSI Hoek-Brown criterion relationships. Int J Rock Mech Min Sci 89:185–199

Bieniawski ZT (1973) Engineering classifications of jointed rock masses. Transactions, South African Institution of Civil Engineer 15:335–345

Chen DF, Xu DP, Ren GF, Jiang Q, Liu GF, Wan LP, Li N (2019) Simulation of cross-correlated non-Gaussian random fields for layered rock mass mechanical parameters. Comput Geotech 112:104–119

Chen FF (2004) A method of elastoplastie back analysis by emulating construction of tunnel. Xi'an: Xi'an University of Technology

China metallurgical construction association (2015) Technical code for engineering of ground anchorages and shotcrete support (GB50086-2015). China Planning Press, Beijing

Gao LY, Yu GM, Zhao JF, Wan XM, Yuan CF (2016) Analysis and application of yielding approach based on material strength criteria. Journal of Chongqing University 39:73–81

Gokceoglu C, Sonmez H, Kayabasi A (2003) Predicting the deformation moduli of rock masses. Int J Rock Mech Min Sci 40(5):701–710

Guo XF, Yan EC, Wu XC, Yin JM, He PT (2014a) Research on shear strength characteristics of slope rock mass on project of water diversion from Han to Wei River project. Chin J Rock Mechan Eng 35:3589–3594

Guo XF, Yan EC, Wu XC, Yin JM, Zhou CH (2014b) Study of deformation characteristics of slope rock mass at project of water diversion

from Hanjiang River to Weihe River. Rock and Soil Mechanics 35:2927–2933

He MM, Li N, Zhang ZQ (2019a) An empirical method for determining the mechanical properties of jointed rock mass using drilling energy. Int J Rock Mech Min Sci 116:64–74

He MM, Zhang ZQ, Ren J, Huan J, Li GF, Chen Y, Li N (2019b) Deep convolutional neural network for fast determination of the rock-strength parameters using drilling data. Int J Rock Mech Min Sci 123:104184

He MM, Zhang ZQ, Zheng J, Chen FF, Li N (2020) A new perspective on the constant m(i) of the Hoek-Brown failure criterion and a new model for determining the residual strength of rock. Rock Mech Rock Eng 53(9):3953–3967

He MM, Zhang ZQ (2021) Li N (2021a) Prediction of fracture frequency and RQD for the fractured rock mass using drilling logging data. Bull Eng Geol Env. https://doi.org/10.1007/s10064-021-02240-3

He MM, Zhang ZQ, Li N (2021b) Deep convolutional neural networks-based method for strength parameter prediction of jointed rock mass using drilling logging data. Int J Geomech. February 2021. https://doi.org/10.1061/(ASCE)GM.1943-5622.0002074

Hobbs DW (1968) Scale model study of strata movement around mine roadways I. The dependence of roadway closure upon rock strength. Int J Rock Mech Min Sci Geomech Abstr 5:219–235

Hobbs DW (1969) Scale model studies of strata movement around mine roadways—IV. Roadway shape and size. Int J Rock Mech Min Sci Geomech Abstr 6:365–404

Hoek E, Brown ET (1980) Empirical strength and criterion for rock masses. J Geotech Eng 106:1013–1035

Hoek E, Carranza-Torres CT, Corkum B (2002) Hoek-Brown failure criterion-2002 edition.In: Bawden HRW, Curran J, Telsenicki M, eds. Proceedings of the Fifth North American Rock Mechanics Society (NARMS-TAC 2002) Symposium. Toronto, Canada: Mining Innovation and Technology 2002: 267–273

Hoek E, Diederichs MS (2006) Empirical estimation of rock mass modulus. Int J Rock Mech Min Sci 43(2):203–215

Hoek E, Marinos PG, Benissi M (1998) Applicability of the geological strength index (GSI) classification for weak and sheared rock masses—the case of the Athens schist formation. Bull Eng Geol Environ 57(2):151–160

Jiang Q, Liu XP, Yan F, Yang Y, Xu DP, Feng GL (2021a) Failure Performance of 3DP Physical Twin-Tunnel Model and Corresponding Safety Factor Evaluation. Rock Mech Rock Eng 54:109–128

Jiang Q, Shi YE, Yan F, Zheng H, Kou YY, He BG (2021b) Reconstitution method for tunnel spatiotemporal deformation based on 3D laser scanning technology and corresponding instability warning. Engi Fail Ana 125:105391

Li N, Chen YS, Chen FF, Zhang ZQ (2006a) Research on tunnel stability criterion. Chin J Rock Mech Eng 25:1941–1944

Li N, Liu NF, Li GF (2014) New method for stability evaluation of soil and soft rock tunnels. Chin J Rock Mech Eng 33:1812–1821

Li N, Liu NF, Zhang CK, Jian Q (2015) Fast analysis and design methods for stability of city gate tunnels under complicated geological conditions. Chin J Rock Mech Eng 34:1435–1443

Li N, Luo JZ, Chang B, Zhang ZQ (2006b) New method for design and analysis of underground caverns. Chin J Rock Mech Eng 25:2155–2159

Li N, Yang M, Li GF (2019) Revisiting on the application of finite element method in geotechnical engineering. Rock and Soil Mechanics 40:1–10

Li WJ, Zhu YQ (2013) Tunnel mechanics. China Machine Press, Beijing, China

Li Y, Zhou GY, Tang CA, Wang SY, Wang KK, Wang TT (2021) Influence of undercrossing tunnel excavation on the settlement of a metro station in Dalian. Bull Eng Geol Environ 80:4673–4687

Liu NF, Li N, Li GF, Ran JX, Deng BY (2015) Analysis of the collapse mechanism of the kuyu water conveyance tunnel and assessment of the effectiveness of its ground reinforcements. Chin J Rock Mech Eng 34:2531–2541

Liu TH, Wang L, Li L, Yang F, Chen ZW, Liu HK (2021) Pressure waves acting on wall of a tunnel and their impact on the tunnel's structural safety. Journal of Central South University 28:3223–3237

Ma K, Xu J, Wu SG, Zhang AH (2009) Research on surrounding rock stability in local collapse section of highway tunnels. Rock and Soil Mechanics 30:2955–2960

Ma ZT, Tan YL (2005) Simulation study of rock failure based on MH-PCA model. Chinese Journal of Mechanical Engineering 24:2704–2708

Mitri HS, Edrissi R, Henning J (1994) Finite element modelling of cable-bolted stopes in hardrock groundmines. SME Annual Meeting. Albuquerque. New Mexico 1994:94–116

Muhammad RA, Malcolm G, Sean PR (2019) Numerical simulation of the impact of geological heterogeneity on performance and safety of THAI heavy oil production process. J Petrol Sci Eng 173:1130–1148

Nicholson GA, Bieniawski ZT (1990) A nonlinear deformation modulus based on rock mass classification. Int J Min Geol Eng 8(3):181–202

Ong DEL, Choo CS (2018) Assessment of non-linear rock strength parameters for the estimation of pipe-jacking forces. Part 1. Direct shear testing and backanalysis. Eng Geol 244:159–172

Pi ZP, Xiao JQ, Hu HP (2015) Simulation of rock failure with MH-PCA model based on principle of energy dissipation. Journal of Disaster Prevention and Mitigation Engineering 34:235–241

Read SAL, Richards LR, Perrin ND (1999) Applicability of the Hoeke Brown failure criterion to New Zealand greywacke rocks. Proceedings of the 9th International Congress on Rock Mechanics. Paris. 1999:655–660

Ren JX (2017) Finite element analysis on surrounding rock stability of Qinling Tunnel for Hanjiang-to-Weihe River Valley Water Diversion Project. Water Resources and Hydropower Engineering 48:55–58

Serafim JL, Pereira JP (1983) Consideration of the geomechanical classification of Bieniawski. Proceedings of International Symposium on Engineering Geology and Underground Construction. Rotterdam: A.A. Balkema. II 1983:3–44

Sonmez H, Gokceoglu C, Nefeslioglu HA, Kayabasi A (2006) Estimation of rock modulus: for intact rocks with an artificial neural network and for rock masses with a new empirical equation. Int J Rock Mech Min Sci 43(2):224–235

Sonmez H, Gokceoglu C, Ulusay R(2004) Indirect determination of the modulus of deformation of rock masses based on the GSI system. Int J Rock Mech Min Sci 41(5):849–857

Wang ZJ, Gao JY, Zhang P, Guan X, Ji XF (2019) Stability analysis of tunnel face in high-pressure karst tunnels based on catastrophe theory. Chin J Geotech Eng 41:95–103

Yan X, Kulatilake PHSW, Sandbak LA (2018) Effect of rock mass and discontinuity mechanical properties and delayed rock supporting on tunnel stability in an underground mine. Eng Geol 238:62–75

Yu X, Zheng Y, Liu H, Fang Z (1983) Stability analysis of surrounding rocks in underground engineering. China Coal Industry Publishing House, Beijing

Zhang C (2015) Elastoplastic analytical solution of underground tunnel under non-axisymmetric conditions. Xi'an University of Technology, Shaanxi

Zhang LY, Einstein HH (2004) Using RQD to estimate the deformation modulus of rock masses. Int J Rock Mech Min Sci 41:337–341

Zhang XP, Jiang YJ, Sugimoto S (2019) Anti-plane dynamic response of a non-circular tunnel with imperfect interface in anisotropic rock mass. Tunn Undergr Space Technol 87:134–144

Zhang ZQ, Chen FF, Li N, Swoboda G, Liu NF (2017) Influence of fault on the surrounding rock stability of a tunnel: Location and thickness. Tunn Undergr Space Technol 61:1–11